https://doi.org/10.5194/egusphere-2022-786
Preprint. Discussion started: 26 August 2022

Development of an ecophysiology module in the GEOS-Chem chemical transport model version 12.2.0 to represent biosphere–atmosphere fluxes relevant for ozone air quality

Joey C. Y. Lam[1], Amos P. K. Tai[1,2], Jason A. Ducker[3,4], and Christopher D. Holmes[3]

[1] Earth System Science Programme and Graduate Division of Earth and Atmospheric Sciences, Faculty of Science, The Chinese University of Hong Kong, Sha Tin, Hong Kong
[2] State Key Laboratory of Agrobiotechnology, and Institute of Environment, Energy and Sustainability, The Chinese University of Hong Kong, Sha Tin, Hong Kong
[3] Department of Earth, Ocean and Atmospheric Science, Florida State University, Tallahassee, Florida, USA
[4] Lynker Technologies, LLC, Leesburg, Virginia, USA

Correspondence to: Amos P. K. Tai (amostai@cuhk.edu.hk)

Abstract. Ground-level ozone (O_3) is a major air pollutant that adversely affects human health and agricultural productivity. Removal of air pollutants including tropospheric O_3 from the atmosphere by vegetation is controlled mostly by the process of dry deposition, an important component of which is plant stomatal uptake that can in turn cause damage to plant tissues with ramifications for ecosystem and crop health. In many atmospheric and land surface models, the openness of plant stomata is represented by a bulk stomatal conductance, which is often semi-empirically parameterized , and highly fitted to historical observations. A lack of mechanistic linkage to ecophysiological processes such as photosynthesis may render models insufficient to represent plant-mediated responses of atmospheric chemistry to long-term changes in CO_2, climate and short-lived air pollutant concentrations. A new ecophysiology module was thus developed to mechanistically simulate land–atmosphere exchange of important gas species in GEOS-Chem, a chemical transport model widely used in atmospheric chemistry studies. We adopted the formulations from the Joint UK Land Environmental Simulator (JULES) to couple photosynthesis rate, bulk stomatal conductance and isoprene emission rate dynamically. The implementation not only allows dry deposition to be coupled with plant ecophysiology, but also enables plant and crop productivity and functions to respond dynamically to atmospheric chemical changes. The research questions of this study include: 1) how the new ecophysiology module compares with the prior, semi-empirical parameterization in terms of simulating concentration and dry deposition velocity of O_3 with respect to site measurement-based estimates; and 2) whether the ecophysiology module simulates vegetation productivity, dry deposition, isoprene emission rate and O_3–vegetation interactions reasonably under a present-day and an elevated CO_2 concentration. We conduct simulations to evaluate the effects of the ecophysiology module on simulated dry deposition velocity and concentration of surface O_3 against an observation-derived dataset known as SynFlux. Our estimated dry deposition velocity of O_3 is close to SynFlux dry deposition velocity with root-mean-squared errors (RMSE) ranging from 0.1 to 0.2 cm s^{-1} across different plant functional types (PFTs), despite an overall positive bias in surface O_3 concentration (by up to 16 ppbv). Representing ecophysiology was found to reduce the simulated biases in deposition fluxes from the prior model, but worsen the

https://doi.org/10.5194/egusphere-2022-786
Preprint. Discussion started: 26 August 2022

positive biases in simulated O_3 concentrations. The increase in positive concentration biases is mostly attributable to the eco-physiology-based stomatal conductance being generally smaller (and closer to SynFlux values) than that estimated by the prior semi-empirical formulation, calling for further improvements in non-depositional processes relevant for O_3 simulations. Estimated global O_3 deposition flux is 864 Tg O_3 yr^{-1} with GEOS-Chem, and the new module decreases this estimate by 92 Tg O_3 yr^{-1}. Estimated global gross primary product (GPP) is 119 Pg C yr^{-1}, with an O_3-induced damage of 4.2 Pg C yr^{-1} (3.5%). An elevated CO_2 scenario (580 ppm) yields higher global GPP (+16.8%) and lower global O_3 depositional sink (–3.3%). Global isoprene emission simulated with a photosynthesis-based scheme is 317.9 Tg C yr^{-1}, which is 31.2 Tg C yr^{-1} (−8.9%) less than that calculated using the MEGAN emission algorithm. This new model development dynamically represents the two-way interactions between vegetation and air pollutants, and thus provides a unique capability in evaluating pollutant impacts on vegetation health and feedback processes that can shape atmospheric chemistry and air quality especially for any timescales shorter than the multidecadal timescale.

1 Introduction

Surface ozone (O_3) is a strong oxidative species and is harmful to human respiratory system (e.g., Anenberg et al., 2010) and vegetation, with ramifications to boundary-layer meteorology (e.g. Sadiq et al., 2017), water and carbon cycle (e.g. Sitch et al. 2007; Lombardozzi et al., 2015), crop production (e.g. Ainsworth et al, 2012; Avnery et al, 2011) and food security (e.g. Tai et al, 2014; Tai and Val Martin, 2017). Tropospheric O_3 is not emitted directly into the atmosphere, but is generated by photochemical oxidation of precursor gases including carbon monoxide (CO), methane (CH_4), and other volatile organic compounds (VOCs) under the presence of nitrogen oxides (NO_x= NO + NO_2); while many of these precursors are mostly from anthropogenic sources, biogenic VOCs (BVOCs) are globally important components of VOCs. The most abundant species of BVOCs is isoprene emitted mostly from land vegetation. Meanwhile, O_3 is mainly removed by chemical loss as well as via dry deposition, whereby vegetation also plays an important role. Therefore, surface O_3 can be significantly modulated by vegetation through isoprene emission and dry deposition. Further, strong positive correlations between surface ozone and temperature have been well documented and attributed to multiple factors including higher isoprene emission and faster decomposition of PAN back to NO_x at higher temperatures (e.g., Jacob and Winner, 2009). Vegetation can therefore further modulate surface O_3 by regulating surface energy balance and surface temperature via transpiration and changing the land surface albedo (e.g., Wang et al., 2020).

Isoprene emission is one of the pathways via which vegetation affects surface O_3 concentration. Isoprene comprises about half of the global BVOC emissions and is mainly produced by terrestrial vegetation. It can be photochemically oxidized under the presence of NO_x to form surface O_3. Therefore, in a VOC–limited environment, more surface O_3 is produced following an increase in isoprene emission rate. However, in a NO_x–limited environment, isoprene can reduce O_3 concentration either by directly reacting with O_3 or sequestrating NO_x as isoprene nitrate (e.g., Sanderson et al., 2003; Tai et al., 2013). An increase in isoprene emission rate could thus reduce surface O_3 concentration. Isoprene emission rate is dependent on both the

https://doi.org/10.5194/egusphere-2022-786
Preprint. Discussion started: 26 August 2022

vegetation type and a complex array of environmental variables, such as sunlight, temperature, soil moisture, and ambient CO_2 concentration. Many previous studies have used various models to estimate the global biogenic isoprene emission budget (e.g., Arneth et al., 2007; Pacifico et al., 2011; Guenther et al., 2012; Unger, 2013), which is about 300–500 Tg C yr^{-1}.

Dry deposition is a process whereby gases and particles in the atmosphere adhere to or are absorbed by any surface via gravitational settling or turbulent transfer. It is often modeled by a resistor-in-series model, analogous to the concept of electric circuit (Wesely, 1989). Under this framework, gaseous species in the atmosphere will go through different layers of air before depositing on a surface, and the flux across each layer is controlled by a resistance. There are three major resistances in this scheme: aerodynamic resistance (r_a), quasilaminar sublayer resistance (r_b) and surface resistance (r_c). For a vegetated surface, r_c is further divided into different components to represent the uptake via different parts of plant canopy and soil surface. The bulk canopy stomatal resistance r_s, which describes the bulk property of plant stomata, is frequently the component that contributes the most to the variability of r_c. Plants modulate their stomata to maximize CO_2 capture and minimize water loss, so stomatal behavior is tightly connected to photosynthesis and depends on environmental conditions such as photosynthetically active radiation (PAR), humidity, temperature, and soil moisture. The openness of stomata is represented by the stomatal conductance, g_s, which is the reciprocal of r_s. The bulk canopy stomatal conductance aggregates the behavior of all stomata inside a canopy. Therefore, smaller resistance or larger conductance represents more open stomata inside a canopy and allows a larger material flux, and vice versa. In many chemical transport models (CTMs), the response of r_s to environmental variables is not fully captured. For example, the parameterization of r_s in Wesely (1989) as commonly implemented in various CTMs includes the dependence on PAR and temperature only. However, atmospheric moisture content is also an essential factor contributing to the variability of r_s. Franks and Farquhar (1999) showed that a doubling of vapor pressure deficit (VPD) reduces r_s by more than 20%. Kavassalis and Murphy (2017) showed that VPD is a strong predictor of midday O_3 in the US, suggesting that vegetation alters O_3 concentration through stomatal regulation. Various mechanistic approaches that include VPD in the formulation of r_s have been suggested (e.g., Leuning, 1995; Medlyn et al., 2011; De Kauwe et al., 2015). These formulations are ultimately connected to the modeling of plant ecophysiology.

Ecophysiology refers to the study of interactions between physiological processes of plants and the environment. Photosynthesis fixes atmospheric CO_2 into terrestrial ecosystems and thereby facilitates the exchange of water, CO_2 and energy between plants and the environment. Formulations to model photosynthesis have been developed by Collatz et al. (1991) and Collatz et al. (1992) for C_3 and C_4 plants, respectively, and widely used in different numerical models (e.g. Sellers et al., 1996; Clark et al. 2011). When plant stomata open to absorb CO_2, water vapor diffuses from the leaf interior to the atmosphere in the process known as transpiration, with ramifications for canopy micrometeorology and boundary-layer meteorology. Stomatal behavior is regulated by a compromise between photosynthetic pathways and transpiration. Larger stomatal conductance results in larger photosynthetic uptake of CO_2 but also larger water loss through transpiration, and plants have evolved to strike a balance between the two. The coupling between photosynthesis and stomatal conductance also has implications for their interactions with the environment under dry conditions. For instance, during a drought event, stomatal conductance decreases

https://doi.org/10.5194/egusphere-2022-786
Preprint. Discussion started: 26 August 2022

as plants attempt to reduce water loss. This, in turn, amplifies the drought condition and reduces ecosystem productivity (e.g., Emberson et al., 2013). Plant stomatal behavior also affects biosphere–atmosphere exchange of other gaseous species relevant for atmospheric chemistry. Besides the exchange of water and CO_2, dry-depositing gaseous species including O_3, sulfur dioxide (SO_2) and hydrogen peroxide (H_2O_2) can be removed from the atmosphere through plant stomata. Thus, the openness of plant stomata affects the dry deposition flux of these gaseous species, altering concentrations of near-surface air pollutants. For example, O_3 dry deposition is suppressed during drought events, possibly resulting in higher surface O_3 concentrations (Emberson et al., 2013; Huang et al., 2016).

O_3–vegetation interaction is another important topic in plant ecophysiology that is also relevant for atmospheric chemistry. Vegetation not only affects O_3 but is also influenced by O_3, which can attack and damage plant tissues upon stomatal uptake. When the O_3 flux into plant stomata is small, plants naturally detoxify the oxidative stress from O_3, but large O_3 flux overwhelms the detoxification capacity and may cause visible foliage injury. Stomata can close, or in some cases become "sluggish" in responding to environmental changes (e.g., Huntingford et al., 2018), as a result of O_3 damage, with ramifications to boundary-layer meteorology, water and carbon cycle, crop production and food security. In particular, it reduces gross primary production (GPP), which is the gross carbon uptake via photosynthesis and a measure of ecosystem productivity. O_3-induced reduction in GPP is usually less than 10% globally under present-day O_3 concentration, but it can be more than 30% regionally (Lombardozzi et al., 2015; Yue and Unger, 2015). Stomatal control of O_3 uptake also appears to explain the divergent trends in O_3 concentration and plant damage in the recent decade (Ronan et al., 2020). Overall, there are three major feedback pathways that couple surface O_3 to vegetation, whereby O_3 damage on vegetation ultimately affects O_3 itself (Sadiq et al., 2017; Zhou et al., 2018; Wang et al., 2020). First, long-term decline in GPP and leaf area index (LAI) due to O_3 damage can suppress BVOC emissions, thereby modulating surface O_3; in a high-NO_x environment, this may reduce O_3 levels, constituting a negative feedback. Second, O_3 damage generally reduces stomatal conductance and thus the dry-depositional flux of O_3, thereby enhancing surface O_3 concentration (i.e., positive feedback). Finally, O_3 damage can suppress transpiration and the associated evaporative cooling effect, thereby enhancing surface temperature and surface O_3 (i.e., positive feedback).

Rising CO_2 can further complicate O_3–vegetation interactions. An elevated CO_2 concentration alters plant behaviors and thus atmospheric chemistry via three main pathways. First, plants tend to close their stomata more as the CO_2 diffusive flux increases, and such stomatal responses to changing CO_2 can be described either mechanistically (e.g., Clark et al., 2011) or empirically (e.g., Franks et al., 2013). Dry deposition flux is thus reduced, and the corresponding chemical gas species remain in the atmosphere longer. For example, Sanderson et al. (2007) suggested that O_3 concentration could increase by 8 ppbv under a doubling of present-day CO_2 concentration due to reduced stomatal conductance and dry deposition. A reduction in dry deposition flux of O_3 should imply less O_3 damage on plants, but more O_3 left in the atmosphere in the longer term might offset such benefit. Second, it was shown that isoprene emission can be suppressed by elevated CO_2 (Possell and Hewitt, 2011). In high-NO_x environments, lower isoprene emission reduces O_3 production rate, but in NO_x-limited regions such as tropical forests and other remote areas, O_3 concentration may increase (Tai et al., 2013). Finally, higher CO_2 enhances

https://doi.org/10.5194/egusphere-2022-786
Preprint. Discussion started: 26 August 2022

photosynthesis and thus LAI in the long term, and this is known as CO_2 fertilization. This can enhance both dry deposition and isoprene emission, either enhancing or offsetting the previous two effects depending on the O_3 formation regime.

In view of the above, a proper representation of ecophysiological processes has the potential to improve atmospheric chemistry modeling, especially in relation to biosphere-atmosphere exchange. This can be done in various ways. A CTM can be coupled with a land surface or biosphere model within an Earth system framework, whereby atmospheric processes (e.g., deposition, emissions) can be linked dynamically to biospheric processes (e.g., photosynthesis, stomatal regulation, soil biogeochemistry). For instance, Sadiq et al. (2017) and Lei et al. (2020) both examined O_3-vegetation interactions by developing a modeling framework where ozone air quality, ecophysiology and ecosystem structure (e.g., LAI, canopy height) can co-evolve interactively. This approach is particularly useful for examining how ecosystem structure may respond to long-term atmospheric chemical changes over multidecadal timescales, but may be unnecessarily computationally expensive for problems involving shorter timescales, e.g., seasonal responses of plant-atmosphere interactions and O_3 pollution to droughts or heatwaves (e.g., Emberson et al., 2013). It also introduces extra uncertainties that arise from the computation of ecosystem structure, which involves complex representation of plant phenology and biogeochemistry (e.g., allocation, biomass growth, senescence, mortality), while not necessarily improving model performance in atmospheric chemistry. A more efficient approach is to implement process-based representation of ecophysiology into a CTM. This has been done to various extents in the past; e.g., Zhang et al. (2003) implemented a semi-empirical, multiplicative scheme based on Jarvis (1976) to account for plant responses to varying radiation, temperature, VPD, and soil water stress. However, thus far the variability of r_s is still often not fully captured in CTMs. A mechanistic approach in modeling r_s should account for the ecophysiology behind, especially photosynthesis, and therefore better simulate r_s.

In this study, we developed a new ecophysiology module in the GEOS-Chem chemical transport model to dynamically simulate bulk canopy stomatal conductance g_s and plant photosynthesis A_n. Figure 1 summarizes the interactions in the prior GEOS-Chem and in the new ecophysiology module. We highlight that O_3 damage on vegetation is a key component in the model because it allows atmospheric chemistry, in addition to meteorology, to affect plant ecophysiology, and represents a more complete set of two-way interactions and feedback pathways. This development not only provides an alternative to the prior parameterization in the dry deposition module based on Wesely (1989), but also allows biogeoscientists to study the effects of pollutant deposition on plant health, especially when simultaneously influenced by other stresses such as droughts and heatwaves. By considering leaf biochemistry, boundary-layer meteorology, soil moisture stress and O_3 deposition damage, this new module can couple physiological processes to atmospheric chemistry, and with it. We particularly aim to address two questions:

1. How does the ecophysiology module compare to the semi-empirical Wesely (1989) parameterization in terms of simulating concentration and dry deposition velocity of O_3, when compared to estimates based on site measurements?
2. Does the ecophysiology module simulate vegetation productivity, dry deposition, isoprene emission rate and O_3–vegetation interactions reasonably under a present-day and an elevated CO_2 concentration?

https://doi.org/10.5194/egusphere-2022-786
Preprint. Discussion started: 26 August 2022

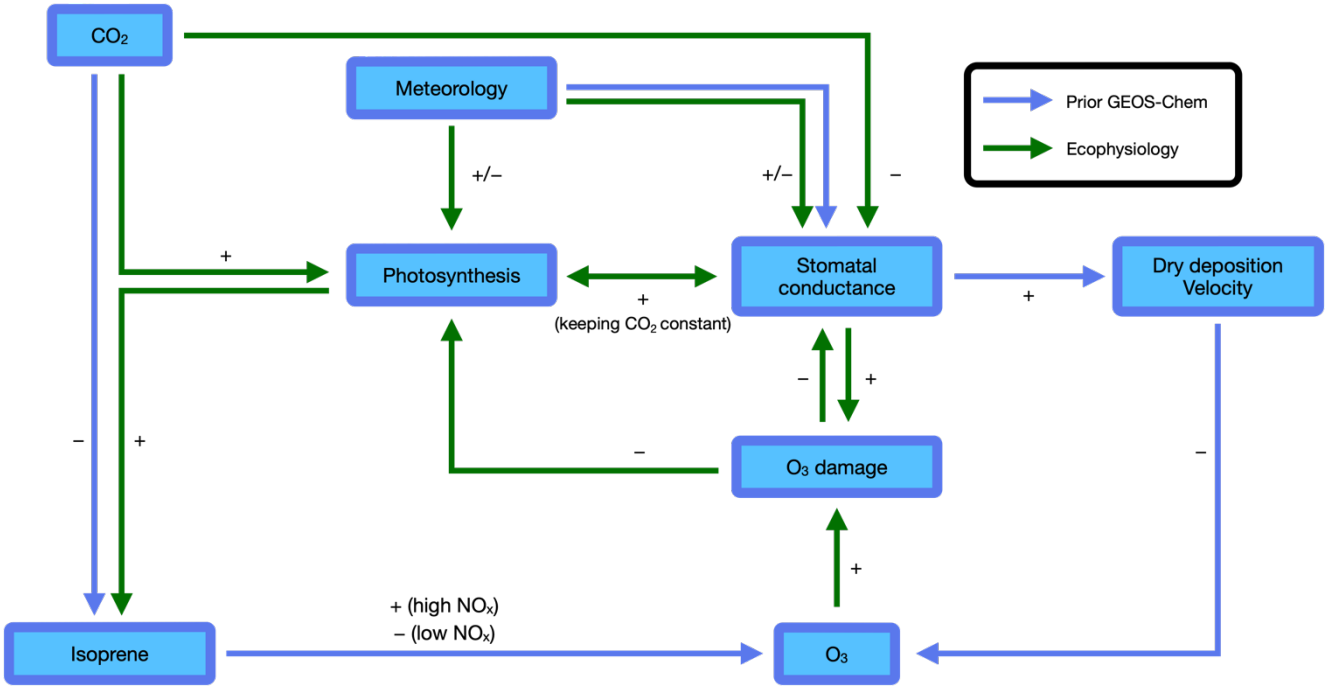

Figure 1: Atmosphere–biosphere interactions represented in the GEOS-Chem chemical transport model. Blue arrows indicate interactions included in the prior GEOS-Chem without ecophysiology. Green arrows indicate interactions added in the new ecophysiology module. The sign associated with each arrow indicates the sign of effect of one factor on another. The two arrows pointing from "Meteorology" to "Stomatal conductance" indicate that the ecophysiology module changes how meteorology affects stomatal conductance. Other species are also simulated by the GEOS-Chem and may interact with O_3, but are omitted here for simplicity.

2 Model

2.1 Model description

The GEOS-Chem global chemical transport model (www.geos-chem.org) version 12.2.0 includes detailed HO_x–NO_x–VOC–O_3–halogen–aerosol tropospheric chemistry (Bey et al., 2001). We conducted simulations at a horizontal resolution of 2° latitude by 2.5° longitude, driven by assimilated meteorology at an hourly time resolution from the Modern-Era Retrospective analysis for Research and Applications, Version 2 (MERRA-2) (Gelaro et al., 2017) dataset, which is an atmospheric reanalysis dataset that includes assimilation of aerosol observations. Leaf area indices (LAI) are prescribed by a gridded dataset from Yuan et al. (2011), who used gap-filling and smoothing techniques to process MODIS (Moderate Resolution Imaging Spectroradiometer) LAI. Emission data are handled by the Harmonized Emission Component (HEMCO) v2.1 (Keller et al., 2014). HEMCO uses anthropogenic emissions of CO, NO_x and non-methane VOCs (NMVOCs) from the Community Emissions Data System (CEDS) inventory (Hoesly et al., 2018) and the biogenic emissions of NMVOCs are computed by the Model of Emissions of Gases and Aerosols from Nature (MEGAN) version 2.1 (Guenther et al., 2012). Besides the MEGAN emission inventory, we also implemented a photosynthesis-based isoprene emission scheme following Pacifico et al. (2011) as an

https://doi.org/10.5194/egusphere-2022-786
Preprint. Discussion started: 26 August 2022

alternative. The scheme introduces another pathway of coupling atmospheric chemistry to ecophysiology. The detailed formulation is included in Sect. 2.1.8.

Dry deposition is modeled using the Wesely (1989) scheme, but with r_s calculated from the new ecophysiology module. It is simulated for every land surface type in the Olson Land Map, which is derived from the USGS global land characteristics database (https://doi.org/10.5066/F7GB230D). These land surface types are also mapped into five plant functional types (PFTs), which are used in the ecophysiology module to represent different types of vegetation. The five PFTs are broadleaf tree, needleleaf tree, C_3 grass, C_4 grass, and shrub. Each PFT has a different set of parameters, thus yielding different r_s. PFT-specific parameters (tabulated in Table S1) are from Clark et al. (2011), Raoult et al. (2016) and Sitch et al. (2007). The module would skip the calculation for a PFT if it does not exist within the grid cell. The ecophysiology module also requires extra soil parameters to calculate soil moisture stress (see Sect. 2.1.5). We used gridded soil parameter data from the Hadley Centre Global Environment Model version 2 – Earth System Model (HadGEM2-ES) to calculate the soil moisture stress function (details in Sect. 2.1.5). Besides r_s, vegetation-related outputs such as gross photosynthetic uptake of carbon, canopy dark respiration and canopy O_3 uptake are also available. The formulations in the ecophysiology module were adopted from the Joint UK Land Environmental Simulator (JULES) (Best et al., 2011; Clark et al., 2011) and are detailed below.

2.1.1 Leaf biochemistry

Photosynthesis consists of two main stages: the light reaction, where energy from sunlight is harnessed to form high-energy and electron-carrying intermediate molecules known as adenosine triphosphate (ATP) and reduced nicotinamide adenine dinucleotide phosphate (NADPH), and the dark reaction, where ATP and NADPH produced in the light reaction are used to power the reduction of CO_2 to carbohydrates via a biochemical reaction cycle known as the Calvin cycle. The Calvin cycle can further be separated into three phases. The first phase is carboxylation, where CO_2 molecules enter and combine with ribulose-1,5-bisphosphate (RuBP) into a 3-carbon compound. The rate of carboxylation is controlled by an enzyme known as ribulose bisphosphate carboxylase/oxygenase (Rubisco), and thus this rate is also known as Rubisco-limited rate. The second phase is reduction, where the three-carbon product is reduced by NADPH and ATP to produce glyceraldehyde 3-phosphate (G3P), some of which then exit the Calvin cycle and are used to synthesize other carbohydrates. The remaining G3P molecules are utilized to regenerate RuBP under the presence of ATP in the final phase known as regeneration. The rates of reduction and regeneration are limited by the availability of ATP and NADPH molecules, and ultimately depend on the utilization rate of G3P, also known as the product-limited rate, and the rate of photon-assimilating reactions in the light reaction, also known as light-limited rate. Plants that follow the above mechanism are called C_3 plants, because CO_2 molecules are synthesized into 3-carbon products directly. There are also C_4 plants, which first incorporate CO_2 into a 4-carbon compound, which is then transported to another cell where CO_2 is released and consumed in the dark reaction. Formulations of photosynthesis rates for C_3 and C_4 plants were derived from leaf biochemistry and formulated as in Collatz et al. (1991) and Collatz et al. (1992), respectively. It is calculated from the three potentially limiting rates:

https://doi.org/10.5194/egusphere-2022-786
Preprint. Discussion started: 26 August 2022

1. Rubisco-limited rate:

   CO_2 assimilation is limited by the availability of CO_2 in intercellular space, the kinetic properties of active sites of Rubisco, and/or the available amount of Rubisco. It is modeled as:

$$W_c = \begin{cases} V_{cmax}\left(\frac{c_i - \Gamma}{c_i + K_c\,(1 + o_i\,/\,K_o)}\right) & \text{for } C_3 \text{ plants} \\ V_{cmax} & \text{for } C_4 \text{ plants} \end{cases} \quad (1)$$

   where V_{cmax} is the maximum carboxylation rate (μmol CO_2 m^{-2} s^{-1}), c_i and o_i are the partial pressures (Pa) of CO_2 and O_2 in intercellular space, respectively, Γ is the CO_2 photorespiration compensation point (Pa), and K_c and K_o are the Michaelis−Menten coefficients (Pa) for carboxylation and oxygenation, respectively. c_i is calculated in Sect. 2.1.4. o_i is assumed to be equal to the partial pressure of O_2 in the lowest model level. Detailed formulations of temperature-dependent parameters are included in the supplementary materials.

2. RuBP-limited rate (light-limited rate):

   It describes the regeneration rate of RuBP, which depends on the amount of ATP and NADPH. This ultimately depends on the availability of absorbed photons, and is modeled as:

$$W_l = \begin{cases} \alpha c_\phi \phi \left(\frac{c_i - \Gamma}{c_i + 2\Gamma}\right) & \text{for } C_3 \text{ plants} \\ \alpha c_\phi \phi & \text{for } C_4 \text{ plants} \end{cases} \quad (2)$$

   where α is the quantum efficiency of photosynthesis (mol CO_2 mol^{-1} PAR), c_ϕ = 4.6 μmol PAR J^{-1} is a conversion constant, and ϕ is the absorbed photosynthetically active radiation (PAR, W m^{-2}).

3. Product-limited rate:

   It refers to the rate of transport of photosynthetic products for C_3 plants and PEP carboxylase limitation for C_4 plants. It is modeled as:

$$W_e = \begin{cases} 0.5\,V_{cmax} & \text{for } C_3 \text{ plants} \\ 2 \times 10^4\,V_{cmax}\,(c_i\,/\,P_s) & \text{for } C_4 \text{ plants} \end{cases} \quad (3)$$

   where P_s is the surface air pressure (Pa).

The leaf-level net photosynthesis (A_n, μmol CO_2 m^{-2} s^{-1}) is calculated as a smoothed minimum (see supplementary materials) of the three potentially limiting rates minus dark respiration (R_d, μmol CO_2 m^{-2} s^{-1}):

$$A_n = \min(W_c, W_l, W_e) - R_d \quad (4)$$

where R_d is linearly proportional to V_{cmax} by the dark respiration coefficient f_{dr}:

$$R_d = f_{dr}\,V_{cmax} \quad (5)$$

2.1.2 Photosynthesis as a diffusive flux

The leaf-level net photosynthesis A_n can also be represented as a diffusive flux of CO_2 modulated by the leaf-level stomatal conductance g_{s0} (m s^{-1}). Therefore, we can find g_{s0} using:

$$g_{s0} = \frac{1.6\times10^{-6}\,A_n}{c_c - c_i} R_* T \quad (6)$$

https://doi.org/10.5194/egusphere-2022-786
Preprint. Discussion started: 26 August 2022

where c_c is the canopy CO_2 partial pressure (Pa), 1.6 accounts for different diffusivities of CO_2 and H_2O through leave stomata, $R_* = 8.31$ J K^{-1} mol^{-1} is the universal molar gas constant, and T is the canopy air temperature (K). We assume c_c and T to be equal to the ambient CO_2 concentration and the 2 m temperature respectively.

2.1.3 Canopy scaling

A simple big-leaf approach is applied to scale up leaf-level variables to the canopy-level variables. It is assumed that incident light is attenuated by the canopy according to Beer's law:

$$I(L) = I_0 e^{-kL} \quad (7)$$

where $I(L)$ and I_0 are the irradiance at the height of the canopy with cumulative leaf area index L and at the top of the canopy, respectively, and k is the PAR extinction coefficient of the canopy. It is also assumed that the in-canopy leaf photosynthetic capacity V_{cmax} at different heights vary proportionally to the in-canopy light profile. Therefore, from Eq. (4), (5) and (6), leaf-level net photosynthesis rate A_n, dark respiration rate R_d, and stomatal conductance g_{s0} also follow the same profile. Integrating over the entire canopy, the canopy-level net photosynthesis A_c, respiration R_{dc} and stomatal conductance g_s are given by:

$$A_c = A_n \frac{1 - e^{-kL_c}}{k} \quad (8)$$

$$R_{dc} = R_d \frac{1 - e^{-kL_c}}{k} \quad (9)$$

$$g_s = g_{s0} \frac{1 - e^{-kL_c}}{k} \quad (10)$$

where L_c is the canopy total leaf area index (m^2 m^{-2}).

2.1.4 Stomatal closure parameterization

A third equation by Jacobs (1994) relating c_i and g_s via canopy humidity deficit D (kg$_w$ kg$_a^{-1}$) is included to obtain a closed set of equations for A_n, g_{s0} and c_c. This formulation was discussed in detail by Cox et al. (1998).

$$\frac{c_i - \Gamma}{c_c - \Gamma} = f_0 \left(1 - \frac{D}{D_*}\right) \quad (11)$$

where f_0 and D_* are PFT-specific parameters. D is evaluated as the difference between the saturation specific humidity (kg$_w$ kg$_a^{-1}$) evaluated at leaf temperature T_l and the 2 m specific humidity. We assume a thin leaf boundary layer, T_l would be equal to the 2 m air temperature.

2.1.5 Soil moisture stress

Under dry soil conditions, A_n, R_d and g_{s0} are reduced due to limited availability of water. An extra factor β_t, which ranges from 0 to 1, is multiplied to all three quantities. It is modeled as:

https://doi.org/10.5194/egusphere-2022-786
Preprint. Discussion started: 26 August 2022

$$\beta_t = \begin{cases} 1 & \text{for } \theta > \theta_c \\ \frac{\theta - \theta_w}{\theta_c - \theta_w} & \text{for } \theta_w < \theta \leq \theta_c \\ 0 & \text{for } \theta \leq \theta_w \end{cases} \quad (12)$$

where $\theta = S \times \theta_s$ is the root zone soil moisture, S is the root zone soil wetness (in terms of fraction of soil pore space), and θ_s, θ_c and θ_w are the saturation, critical and wilting soil moisture, respectively. We use the soil ancillary maps that contain θ_s, θ_c and θ_w at 0.5°×0.5° resolution from HadGEM2-ES.

2.1.6 O_3 damage

The O_3 damage scheme in JULES is based on Sitch et al. (2007). When the ambient O_3 concentration is high enough, A_n, R_d and g_{s0} is further reduced due to O_3 damage on plant cells. An O_3 damage factor β_{O3}, which ranges from 0 to 1, is multiplied to the three quantities. The damage factor is given by:

$$\beta_{O_3} = 1 - a \times \max[F_{O_3} - F_{O_3\,crit}, 0] \quad (13)$$

where F_{O3} is the O_3 deposition flux through stomata (nmol m^{-2} s^{-1}), $F_{O3\,crit}$ is the threshold for stomatal O_3 uptake (nmol m^{-2} s^{-1}), and a is the gradient of the O_3 dose response function (nmol^{-1} m^2 s); a and $F_{O3\,crit}$ are PFT-specific parameters. There are two sets of values of a corresponding to "high" and "low" sensitivities. The stomatal O_3 deposition flux is modeled using a flux gradient approach:

$$F_{O_3} = \frac{[O_3]}{r_a + r_b + \kappa_{O_3} r_s} \quad (14)$$

where $[O_3]$ is the molar concentration of O_3 at the lowest model level, r_a is the aerodynamic resistance (s m^{-1}), r_b is the quasi-laminar sublayer resistance, $r_s = 1 / g_s$ is the stomatal resistance, and $\kappa_{O3} = 1.61$ accounts for the relative difference in diffusivities of O_3 and H_2O through leave stomata. Since r_s in equation (14) depends on β_{O3}, equations (13) and (14) can be combined into a quadratic equation and solved analytically to give β_{O3}.

2.1.7 Open vs. closed stomata

It is important to note that open and closed stomata are treated differently in the module. Open stomata follow the processes described above. Closed stomata are assigned a minimum value of stomatal conductance $g_{min} = 10^{-6}$ m s^{-1}. Photosynthesis and O_3 deposition cannot occur, and thus A_n is only affected by R_d and β_t:

$$A_n = -R_d \beta_t \quad (15)$$

Closed stomata are determined by

1. $g_{s0} \leq g_{min}$, which indicates that g_{s0} is close to zero and the associated fluxes can be neglected,
2. $A_n \leq 0$, which indicates that photosynthesis is not effective, and thus plants close the stomata,
3. $D \geq D_*$, which implies $c_i \leq \Gamma$ from Eq. (11), hence there is no net uptake of CO_2 across stomata,
4. $\beta_t = 0$, which implies a dry soil condition inhibiting photosynthesis, or
5. $\phi = 0$, which implies that PAR is not available for photosynthesis.

https://doi.org/10.5194/egusphere-2022-786
Preprint. Discussion started: 26 August 2022

2.1.8 Photosynthesis-dependent isoprene emission

In priorGEOS-Chem, canopy isoprene emission is computed by MEGAN v2.1, which calculates biogenic VOC emissions of various species as functions of canopy-scale PFT-specific emission factors modulated by environmental activity factors to account for changing temperature, light, leaf age and LAI, weighted by the PFT fraction in each grid cell to give the grid cell-level emission fluxes. The activity factors are essentially semi-empirical functions constrained by experimental data, not explicitly linked to mechanistic ecophysiological processes. Here in the ecophysiology module, canopy isoprene emission (E_{isoprene}, kg C m^{-2} s^{-1}) is linked explicitly to photosynthesis, based on Pacifico et al. (2011):

$$E_{\text{isoprene}} = \text{IEF}\ \rho_{\text{leaf}}\ \frac{A_{\text{c}} + R_{\text{dc}}}{(A_{\text{n}})_{\text{st}} + (R_{\text{d}})_{\text{st}}}\ f_{\text{T}}\ f_{\text{CO2}} \quad (16)$$

where IEF is the PFT-specific isoprene emission factor (μg C g dw^{-1} h^{-1}, "dw" means dry weight), i.e., base emission rate of isoprene at the leaf level under standard conditions (i.e., temperature of 30°C, photosynthetically active radiation of 1000 μmol CO_2 m^{-2} s^{-1}, CO_2 concentration of 370 ppm and without any O_3 damage or soil moisture stress), ρ_{leaf} is the dry leaf area density (g dw^{-1} m^{-2}), f_{T} and f_{CO2} are temperature- and CO_2-dependent empirical factors to account for variation with changing temperature and CO_2 level. Variables with subscript "st" are calculated under standard conditions. f_{T} and f_{CO2} are calculated as:

$$f_{\text{T}} = \min\left[e^{a_{\text{T}}(T - T_{\text{st}})}; 2.3\right] \quad (17)$$

$$f_{\text{CO2}} = (c_{\text{i}})_{\text{st}} / c_{\text{i}} \quad (18)$$

where $a_{\text{T}} = 0.1$ K^{-1}, $T_{\text{st}} = 300$ K, c_{i} is the partial pressure of CO_2 in the intercellular space. We note that, as opposed to Pacifico et al. (2011), our model does not capture a reduction in c_{i} following soil moisture limitation because we use prescribed 2 m specific humidity data in the meteorological input to calculate c_{i}. The effect of soil moisture stress on isoprene emission is only captured in the calculation of A_{c} and R_{dc}. This may lead to a lower isoprene emission rate compared to the original scheme, but direct comparison is not possible due to different input meteorology used in our study.

2.2 Experimental design

To evaluate the modeled concentration and dry deposition velocity of O_3, we conduct four one-year simulations from 1 January 2012 to 1 January 2013 using GEOS-Chem v12.2.0 driven by offline MERRA-2 meteorology. Table 1 summarizes the configurations of each simulation. A control case (case 0) uses the GEOS-Chem v12.2.0 with prior input configuration while other three (cases 1a–c) use the modified GEOS-Chem with ecophysiology module turned on. Each of the three cases use different O_3 damage sensitivities. We then compare the modeled concentration and dry deposition velocity of O_3 against site observations. Year 2012 is chosen as the simulation year to maximize the number of observations our results can be evaluated against.

https://doi.org/10.5194/egusphere-2022-786
Preprint. Discussion started: 26 August 2022

Table 1: Configuration of the first set of simulations that evaluate the modeled concentration and dry deposition velocity of ozone (O_3).

Case	[CO_2] (ppmv)	Ecophysiololgy module	O_3 damage scheme and sensitivity
0	390	Off	No O_3 damage applied
1a	390	On	No O_3 damage applied
1b	390	On	Sitch et al. (2007), low sensitivity
1c	390	On	Sitch et al. (2007), high sensitivity

We also conduct a second set of simulations from 1 January 2000 to 1 January 2001 to demonstrate the capability of the new module to simulate changes in plant productivity in response to changing CO_2 and subsequent changes in atmospheric chemistry. Table 2 summarizes the configuration of each simulation. Case 2a is the control experiment where prior configuration from the GEOS-Chem is used. Case 2b simulates the effect of elevated CO_2 on stomatal conductance by using the CO_2–g_s scaling factor described in Franks et al. (2013) (details are included in supplementary materials) and setting the ambient CO_2 concentration to 580 ppm, which is approximately the projected CO_2 concentration around 2050s in a business-as-usual scenario (e.g., Representative Concentration Pathway 8.5). This simple scaling approach has been suggested to investigate how rising CO_2 may affect ozone dry deposition in the future. This now allows us to compare between the new ecophysiology module, which simulates plant responses to rising CO_2 more mechanistically, and the simple CO_2–g_s scaling factor in the context of O_3 concentration and depositional sink. Cases 2c–f are conducted to compare the O_3 depositional sink and concentration to cases 2a–2b, and to investigate how GPP and O_3 depositional sink changes under an elevated CO_2 scenario. Cases 2g–h are duplicates of 2c–d respectively, except that the isoprene emission rates are calculated using a photosynthesis-based scheme from Pacifico et al. (2011) instead of from the prior MEGAN emission inventory. They reveal whether the photosynthesis-based scheme yields a reasonable estimate of global isoprene emission under our model.

Table 2: Configuration of the second set of simulations that investigate gross primary productivity (GPP) and ozone (O_3) concentration under an elevated CO_2 scenario.

Case	[CO_2] (ppmv)	O_3 damage scheme and sensitivity	Stomatal conductance formulation	Isoprene emission
2a	370	No O_3 damage applied	Wesely (1989) parameterization and CO_2 scaling by Franks et al. (2013)	MEGAN v2.1
2b	580	No O_3 damage applied	Wesely (1989) parameterization and CO_2 scaling by Franks et al. (2013)	MEGAN v2.1

https://doi.org/10.5194/egusphere-2022-786
Preprint. Discussion started: 26 August 2022

2c	370	No O_3 damage applied	Ecophysiology module	MEGAN v2.1
2d	370	Sitch et al. (2007), high sensitivity	Ecophysiology module	MEGAN v2.1
2e	580	No O_3 damage applied	Ecophysiology module	MEGAN v2.1
2f	580	Sitch et al. (2007), high sensitivity	Ecophysiology module	MEGAN v2.1
2g	370	No O_3 damage applied	Ecophysiology module	Photosynthesis-based scheme by Pacifico et al. (2011)
2h	370	Sitch et al. (2007), high sensitivity	Ecophysiology module	Photosynthesis-based scheme by Pacifico et al. (2011)

2.3 Evaluation data: SynFlux

We evaluate the modeled dry deposition velocity and concentration of O_3 against an observationally derived dataset known as Synthetic O_3 Flux (SynFlux) (Ducker et al., 2018). It derives site-level v_d by combining eddy covariance measurements of micrometeorological flux from FLUXNET sites in the United States and Europe with a gridded dataset of O_3 concentration. The aerodynamic and quasilaminar sublayer resistances r_a and r_b from each of the sites are derived from the meteorological quantities measured at the sites. The surface conductance (reciprocal of resistance) is a summation of two components: stomatal conductance g_s and non-stomatal conductance g_{ns}; g_s is derived from the measured water vapor flux and meteorological data, and g_{ns} is estimated using Zhang et al. (2003). Figure 2 shows the locations of 36 SynFlux sites used in our evaluation of the ecophysiology module. The total number of sites for each PFT is listed in the legend of Fig. 2. There are only two sites that represent C_4 grass, and they are ignored because observational data are only available in August. The errors in SynFlux have been shown to be modest compared with differences between observations and regional and global CTMs that are frequently a factor of two or more, illustrating its utility for evaluating models (Ducker et al., 2018).

https://doi.org/10.5194/egusphere-2022-786
Preprint. Discussion started: 26 August 2022

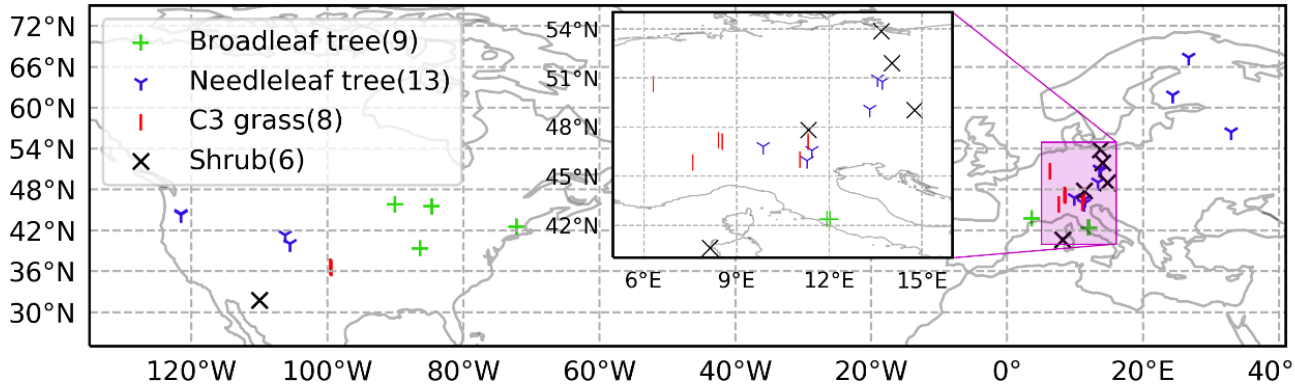

Figure 2: Locations of 36 SynFlux sites used in evaluation of the ecophysiology module. Different symbols indicate different plant functional types (PFTs) as broadleaf tree (Green "+", includes evergreen broadleaf tree (EBF) and deciduous broadleaf tree (DBF)), needleleaf tree (Blue "Y", includes evergreen needleleaf tree (ENF) only), C_3 grass (Red "|", includes grassland (GRA) only), and shrub (Black "X", includes wetland (WET), open shrubland (OSH) and closed shrubland (CSH)). Number of sites for each PFT is bracketed in the legend. Two C_4 grass (including savanna (SAV) and woody savanna (WSA)) sites are ignored in our evaluation due to a lack of observational data in our simulation period. Mixed forest (MF) and cropland (CRO) sites are not classified into any of the PFTs because they are usually composed of multiple PFTs.

3 Results

3.1 Comparison between ecophysiology module and prior Wesely (1989) parameterization

We compare the modeled PFT-specific dry deposition velocity v_d of O_3 in summer (JJA) to SynFlux. The modeled v_d was obtained by averaging hourly outputs of v_d from June to August 2012. It was then paired up with the SynFlux dataset by matching the month, location and PFT. In Fig. 3, the model results on model grid cells closest to the SynFlux sites are plotted against the corresponding observation-derived estimates from SynFlux for each PFT. C_4 grass is ignored due to a lack of observational data. The soil moisture stress factor β_t on the corresponding model grid is represented by the color of the circle.

The ecophysiology module reduces the overestimation in v_d by the prior dry deposition module, especially for broadleaf trees, for which the root-mean-squared error (RMSE) decreases from 0.48 cm s^{-1} to 0.11 cm s^{-1}. C_3 grass shows a similar change where the RMSE decreases from 0.36 cm s^{-1} to 0.21 cm s^{-1} in case 1c, where high O_3 damage sensitivity is applied. C_3 grass is the most sensitive to O_3 damage among the four PFTs as the modeled v_d varies the most under different O_3 damage sensitivities. For needleleaf tree, the overestimation without the ecophysiology module becomes underestimation, regardless of the sensitivity of O_3 damage. O_3 damage barely affects v_d. The lower v_d as simulated by the ecophysiology module is attributable to the ecophysiology-based stomatal conductance being generally smaller than that estimated by the semiempirical formulation, which was also discussed by Wong et al. (2019). The more significant decreases in v_d for broadleaf trees and needleleaf trees than for other PFTs are only due to the differences in formulations, but not due to any other physical reasons.

https://doi.org/10.5194/egusphere-2022-786
Preprint. Discussion started: 26 August 2022

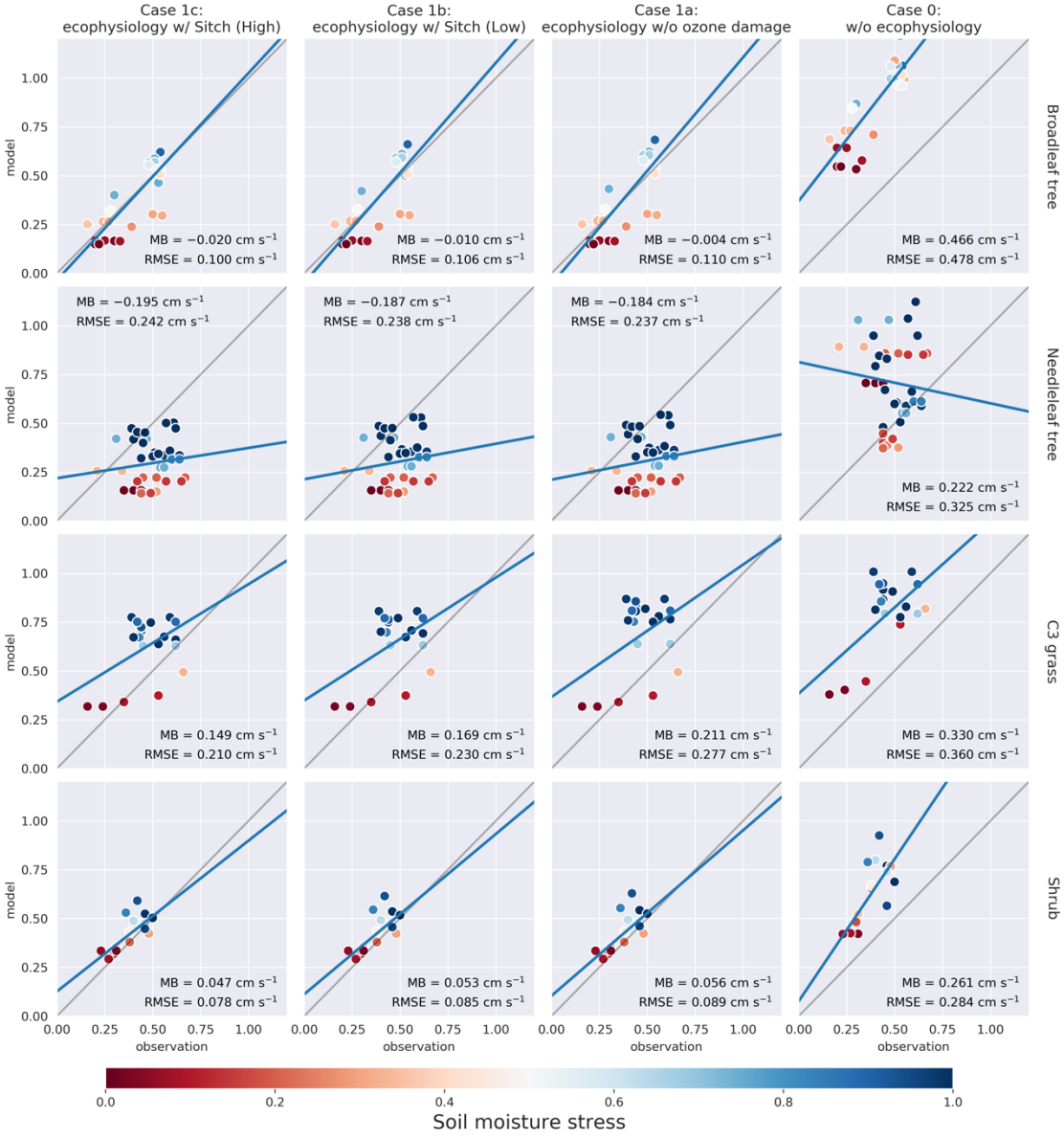

Figure 3: Plots of modeled monthly mean dry deposition velocity of O_3 (cm s^{-1}) in northern summer (JJA) against SynFlux estimates, categorized by site PFT for each simulation case. Columns from right to left represent simulation cases 0, 1a, 1b and 1c. Each row corresponds to a PFT. C_4 grass is ignored due to a lack of observational data. The soil moisture stress factor β_t on the corresponding model grid cell is represented by the color of the circle. Mean bias (MB) and root-mean-squared error (RMSE) are shown for each plot.

In Fig. 3, the colors of circles represent the soil moisture stress factor β_t described in Sect. 2.5. Since the stomatal resistance g_s does not depend on β_t in the semi-empirical parameterization, v_d also does not correlate with β_t. However, v_d

https://doi.org/10.5194/egusphere-2022-786
Preprint. Discussion started: 26 August 2022

simulated using the ecophysiology module is significantly affected by β_t as v_d with low β_t are almost always lower than those with high β_t, regardless of site locations. Also, for broadleaf trees and needleleaf trees, low β_t values appear to result in a nearly constant value of v_d = 0.2 cm s^{-1}, reflecting mostly non-stomatal deposition, while high β_t gives a much closer estimate of v_d to observations. Since g_s is multiplied by β_t as described in Sect. 2.1.5, low β_t values should indeed give lower g_s and thus lower v_d. At different site locations, other components of v_d can also vary, but the strong correlation between β_t and v_d remains. Whether v_d is sensitive to vapor pressure deficit (VPD) in a similar fashion arguably warrants further investigation. Overall, our results indicate that β_t is an important parameter in this formulation and strongly affects the model performance on simulating dry deposition velocity. However, there is a large inter-model variation in β_t due to variability in soil moisture, different formulations of β_t and vertical resolution of soil levels (Trugman et al., 2018). Since GEOS-Chem does not simulate soil explicitly, we only use a simple and empirical parameterization of β_t with input of a single-layer soil moisture from the MERRA-2 dataset. Such deficiency in the representation of β_t may render the model less reliable in simulating the potential impact of drought events on atmospheric chemistry and plant productivity. Therefore, simulation of drought events, which is one of the potential uses of the ecophysiology module, should be interpreted cautiously unless parameters in the β_t function are more thoroughly calibrated on a regional or local basis. Despite the uncertainty of β_t, we emphasize that including the stomatal responses to VPD and soil moisture is valuable because the Wesely (1989) parameterization cannot represent such stomatal responses.

We also compare the model results of monthly mean O_3 concentration in summer with SynFlux estimates, derived from a gridded dataset of O_3 concentration. Figure 4 shows the comparison of monthly mean O_3 concentration on model grid cells closest to the SynFlux sites against the corresponding estimates from SynFlux categorized by site PFT. According to the rightmost column, O_3 concentration is originally overestimated by the GEOS-Chem model. The ecophysiology module increases the model bias by 4 to 5 ppbv for broadleaf trees, needleleaf trees and C_3 grasses, and 2 ppbv for shrubs. Activation of the O_3 damage scheme and the change of sensitivity to O_3 damage only produce modest differences in terms of monthly mean O_3 concentration, representing relatively weak O_3-vegetation feedback effects.

There can be multiple possible reasons leading to the biases in O_3 concentration. First, the simulated O_3 concentration on nearby model grid cells is only a bulk average over the entire area of the grid cell, while the measurement reflects the local O_3 concentration. Subgrid variability created by local meteorology or surface topography is not accounted for during the comparison. Unlike dry deposition velocity, it is not possible to separate O_3 concentration into PFT-specific quantity for a fair comparison. Secondly, accurate simulation of O_3 relies on many non-depositional processes as well, e.g., chemistry, photochemistry, emissions of precursor gases, etc. Since we show that simulation of dry deposition velocity of O_3 is improved by the ecophysiology module, modifications in non-depositional processes would be required more urgently to improve the performance in O_3 simulations. The problems of general overestimation of O_3 by various models at northern midlatitudes have been discussed by Travis et al. (2016).

https://doi.org/10.5194/egusphere-2022-786
Preprint. Discussion started: 26 August 2022

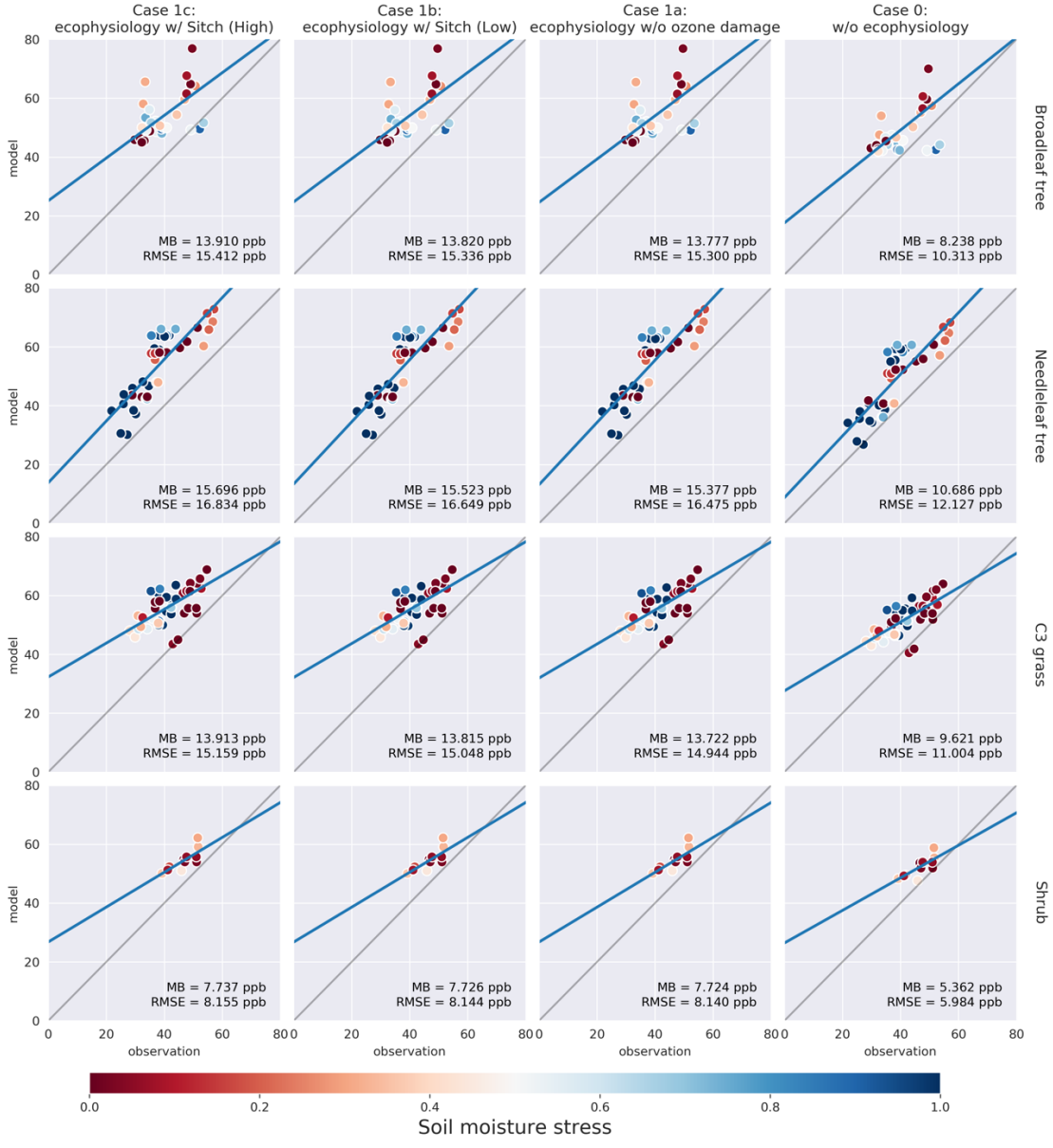

Figure 4: Plots of modeled monthly mean O_3 concentration (ppbv) in northern summer (JJA) against SynFlux data, categorized by site PFT for each simulation case. Columns from right to left represent simulation cases 0, 1a, 1b and 1c. Each row corresponds to a PFT. C_4 grass is ignored due to a lack of observational data. The soil moisture stress factor β_t on the corresponding model grid cell is represented by the color of the circle. Mean bias (MB) and root-mean-squared error (RMSE) is shown for each plot.

https://doi.org/10.5194/egusphere-2022-786
Preprint. Discussion started: 26 August 2022

3.2 GPP and O_3 depositional sink simulated by the ecophysiology module under different CO_2 levels

In the second set of simulations, we demonstrate that with the new dynamic linkage to ecophysiology, the model is capable of capturing CO_2–O_3–vegetation interactions under elevated CO_2 concentration. Table 3 tabulates the global GPP and the O_3 depositional sink for each of the cases, and Figure 5 shows their spatial distributions. Under the year 2000-level CO_2 scenario, the simulated gross primary production (GPP) is 119 Pg C yr^{-1} and the total O_3 depositional sink is 772 Tg O_3 yr^{-1} in the absence of O_3 damage. The global O_3 deposition flux is close to the mean value from 12 CTMs (747 Tg O_3 yr^{-1}) used in the Third Assessment Report of the Intergovernmental Panel on Climate Change (IPCC TAR) (Prather and Ehhalt, 2001), but is generally lower than the values from later multi-model studies (e.g., Stevenson et al., 2006; Wild, 2007; Young et al., 2018). A possible reason is that most CTMs use a semi-empirical formulation of the stomatal conductance, which is generally larger than ecophysiology-based stomatal conductance (Wong et al., 2019), and thus higher dry deposition fluxes in other CTMs are expected. Globally, the O_3 damage on GPP is 4.2 Pg C yr^{-1} (3.5%), but the O_3 damage percentage can reach more than 20% regionally, for example in China, as shown in Fig. 4c.

Table 3: Annual global GPP and total O_3 depositional sink in each simulation.

Case	Global GPP (Pg C yr^{-1})	O_3 depositional sink (Tg O_3 yr^{-1})
2a	N/A	863.6
2b	N/A	812.9
2c	119.0	772.1
2d	114.8	768.1
2e	138.6	746.3
2f	136.0	744.5
2g	119.4	766.4
2h	115.3	761.3

https://doi.org/10.5194/egusphere-2022-786
Preprint. Discussion started: 26 August 2022

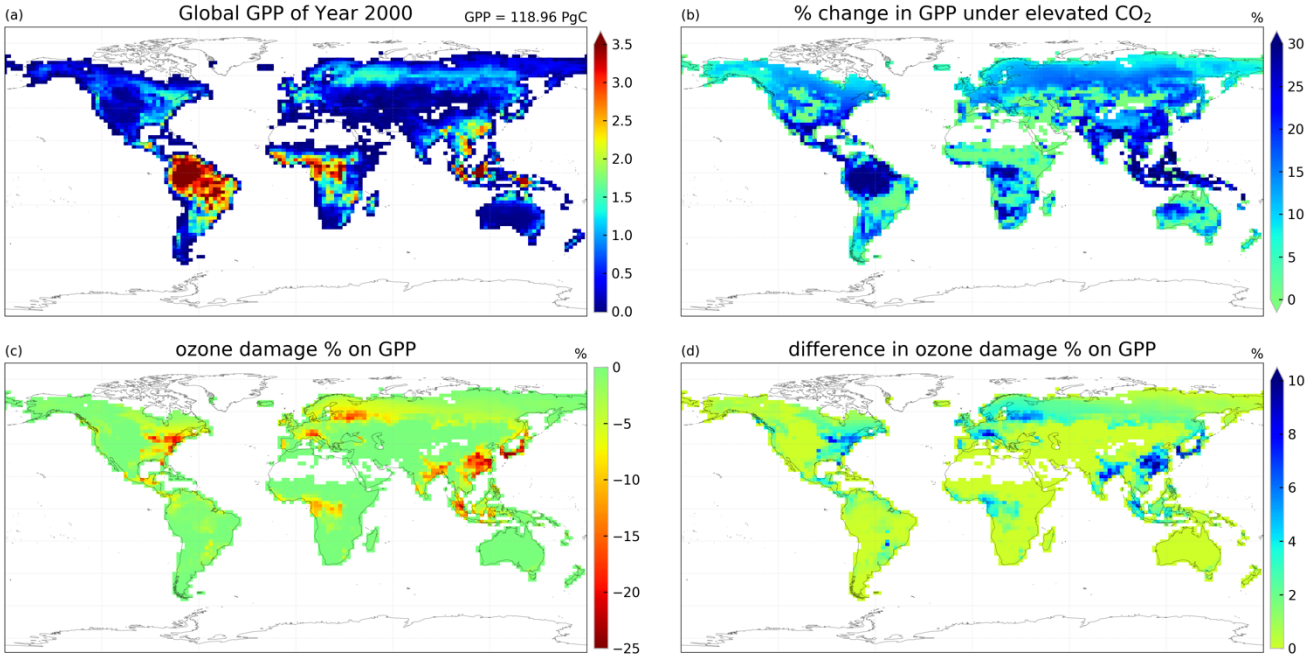

Figure 5a–d: Maps of (a) global GPP distribution (kg C m^{-2} yr^{-1}) in case 2c, (b) percentage change in GPP driven by CO_2 concentration increase, (c) percentage change in GPP driven by high-sensitivity O_3 damage, and (d) difference in O_3-driven percentage change in GPP between experiments with year-2000 and elevated CO_2 concentrations, where the positive values indicate a reduction in ozone damage.

Under elevated CO_2 scenario, GPP is projected to increase by 19.7 Pg C yr^{-1} (16.8%) globally, and up to 30% regionally near tropics (Fig. 5b). We note also that such changes in GPP is entirely due to higher photosynthetic rate, and no changes in LAI are simulated. The global O_3 depositional flux decreases by 25.8 Tg O_3 yr^{-1} (3.3%). This change is about half of that given by the CO_2–g_s scaling factor experiments (cases 2b minus 2a) implying that, compared to the simple CO_2–g_s scaling factor, the mechanistic ecophysiology module predicts less reduction in stomatal conductance at a higher CO_2 level. It should be noted that the simple CO_2–g_s scaling factor is an approximation based only on the RuBP-limited photosynthesis rate (Franks et al., 2013), thus does not necessarily represent the full range of limiting or compensating conditions for photosynthesis. The magnitude of O_3 percentage damage is reduced by around 10% (i.e., the percentage damage goes from about –20% to –10%) in regions with originally high O_3 damage such as southern China, Europe and the eastern US (Fig. 5d). To conclude, it is shown that the model can capture both the direct CO_2 fertilization effect on GPP and the mitigation of O_3 damage under elevated CO_2, leading to higher GPP via both pathways.

The monthly distribution of GPP also generally agrees with results from other models. Figure 6a shows the monthly distribution of global GPP and Fig. 6b–f show the area-weighted average GPP for each of the PFTs. Our results demonstrate a seasonal cycle of GPP that peaks at around 130 g C m^{-2} $month^{-1}$ in July and falls steadily to around 60 g C m^{-2} $month^{-1}$ in February. This resembles with observation-derived datasets like FLUXNET-MTE, as shown in Fig. 3a of Slevin et al. (2017).

https://doi.org/10.5194/egusphere-2022-786
Preprint. Discussion started: 26 August 2022

When the seasonal cycle of GPP for each PFT is considered separately, different trends and features are present. For broadleaf trees, the average GPP stays around 150 to 200 g C m^{-2} $month^{-1}$ throughout a year and is slightly higher in northern summer. C_4 grasses also have a steady average GPP of around 100 to 150 g C m^{-2} $month^{-1}$ but have an opposite cycle to all other PFTs. For needleleaf trees, C_3 grasses and shrubs, GPP is very low in northern winter, but for needleleaf trees, it rises to more than 200 g C m^{-2} day^{-1} in July, which is the highest among all PFTs. Under the elevated CO_2 scenario, GPP is projected to rise by 10 to 30 g C m^{-2} $month^{-1}$, higher in northern summer and vice versa. Most of the increase in GPP can be attributed to broadleaf trees and needleleaf trees, which have larger total leaf surface area than grasses and shrubs, thus amplifying the enhanced photosynthesis under higher ambient CO_2 concentration, as suggested by Eq. (8) in Sect. 2.1.3. On the other hand, C_4 grasses show no change in average GPP throughout a year.

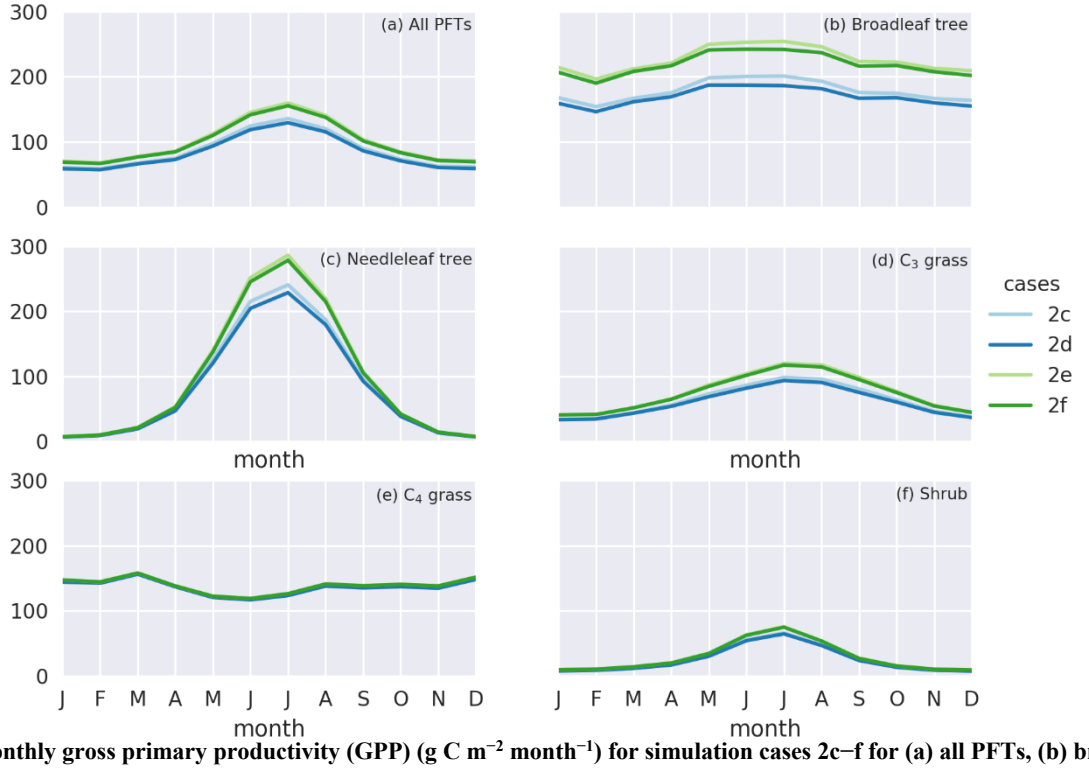

Figure 6a–f: Monthly gross primary productivity (GPP) (g C m^{-2} $month^{-1}$) for simulation cases 2c–f for (a) all PFTs, (b) broadleaf trees, (c) needleleaf trees, (d) C_3 grasses, (e) C_4 grasses and (f) shrubs. Blue and green lines denote simulation cases under year-2000 and elevated CO_2 level respectively. Darker and paler lines denote cases with and without O_3 damage, respectively.

O_3 concentration only changes moderately under elevated CO_2 concentration overall, but with larger changes happening in some regions. Figure 7 shows the change in annual mean O_3 concentration under the increase in CO_2 concentration for cases 2b and 2e. In addition to larger increases of up to 3 ppbv found in the Amazon forest and Borneo regions, smaller

https://doi.org/10.5194/egusphere-2022-786
Preprint. Discussion started: 26 August 2022

increases of up to 1 ppbv are also found in central Africa, Southeast Asia and at middle-high latitudes. This agrees with the simulation result using the CO_2–g_s scaling factor (case 2b). The latter shows even stronger increases in O_3 concentration over the Amazon forest, central Africa and Southeast Asia.

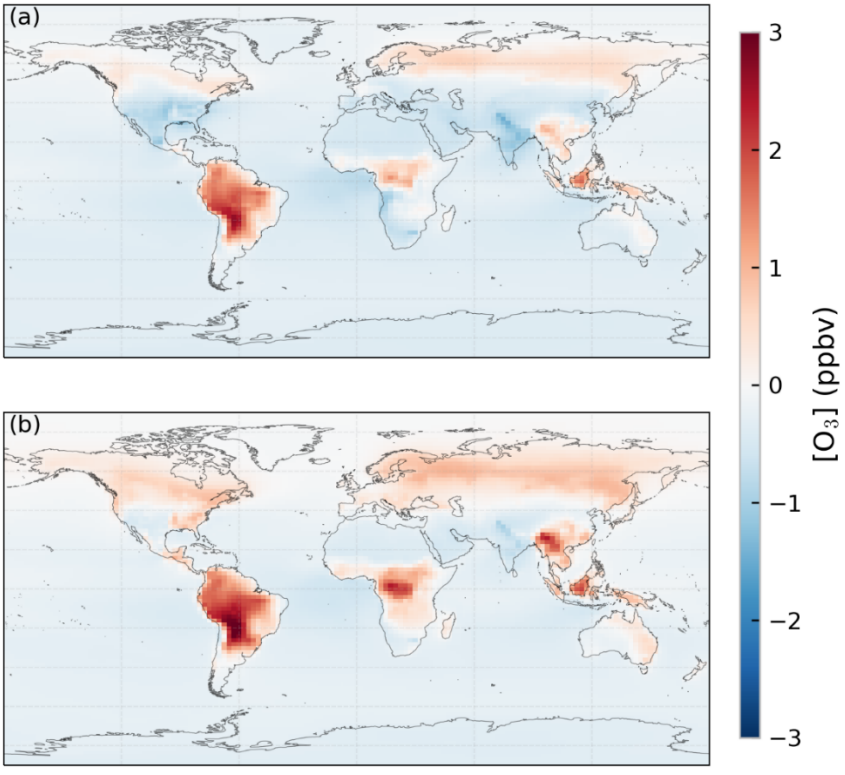

Figure 7a–b: Changes in ozone (O_3) concentration (ppbv) due to the increase in CO_2 concentration simulated using (a) the ecophysiology module and (b) the CO_2–g_s scaling factor.

3.3 Comparison of isoprene emission rates between photosynthesis-dependent formulation and MEGAN v2.1 emission model

Implementing a photosynthesis-dependent isoprene emission scheme into the GEOS-Chem introduces another interaction between ecophysiology and atmospheric chemistry. Here, we demonstrate that the simulated isoprene emission rates are close to what the MEGAN emission algorithm simulates. The annual isoprene emission rates in year 2000 using the MEGAN emission inventory (case 2c) and the photosynthesis-dependent scheme from Pacifico et al. (2011) (case 2g) are shown in Fig. 8a–b, and the annual totals are 349.1 Tg C and 317.9 Tg C respectively. The annual isoprene emission totals are at the lower end of other published estimates of 300–530 Tg C (as summarized in Table 3 in Weng et al., 2020), but are consistent

https://doi.org/10.5194/egusphere-2022-786
Preprint. Discussion started: 26 August 2022

with Weng et al. (2020), who estimated 330–345 Tg C yr^{-1} using the HEMCO v2.1 at a finer spatial resolution than this study. The monthly averages of land surface temperature in year 2000 are lower than the 2000–2009 monthly averages (See Fig. S1), which can lower the emission total. The simulated isoprene emission rate is similar to the MEGAN emission model in general, as the tropics, especially the Amazon forest, contributes the most to the annual isoprene emission total. There are, however, some modest differences in the magnitude and location of the largest emission flux in each of the continents, e.g., from −15 to +10 g C m^{-2} yr^{-1} in different parts of South America, and about −5 g C m^{-2} yr^{-1} in the southern US and Australia. Since the isoprene emission rate is proportional to the photosynthesis rate as in Eq. (16), these differences can be due to the simple classification of PFTs, which can constraint the maximum photosynthesis capacity and thus the photosynthesis rate. We also note that the MEGAN emission model is also subject to uncertainties in its algorithm. Besides, temperature variability in the subgrid scale is often a major source of uncertainty, since a temperature difference of +1°C is equivalent to a +10% increase in isoprene emission rate, as inferred from Eq. (17). Figure 8d shows that global isoprene emission decreases by 12.1 Tg C yr^{-1} (3.8%) (case 2h minus 2g) due to O_3 damage on vegetation. This reduction is mainly due to the 3.5% decrease in GPP via the dry deposition pathway, as described in Sect. 3.2.

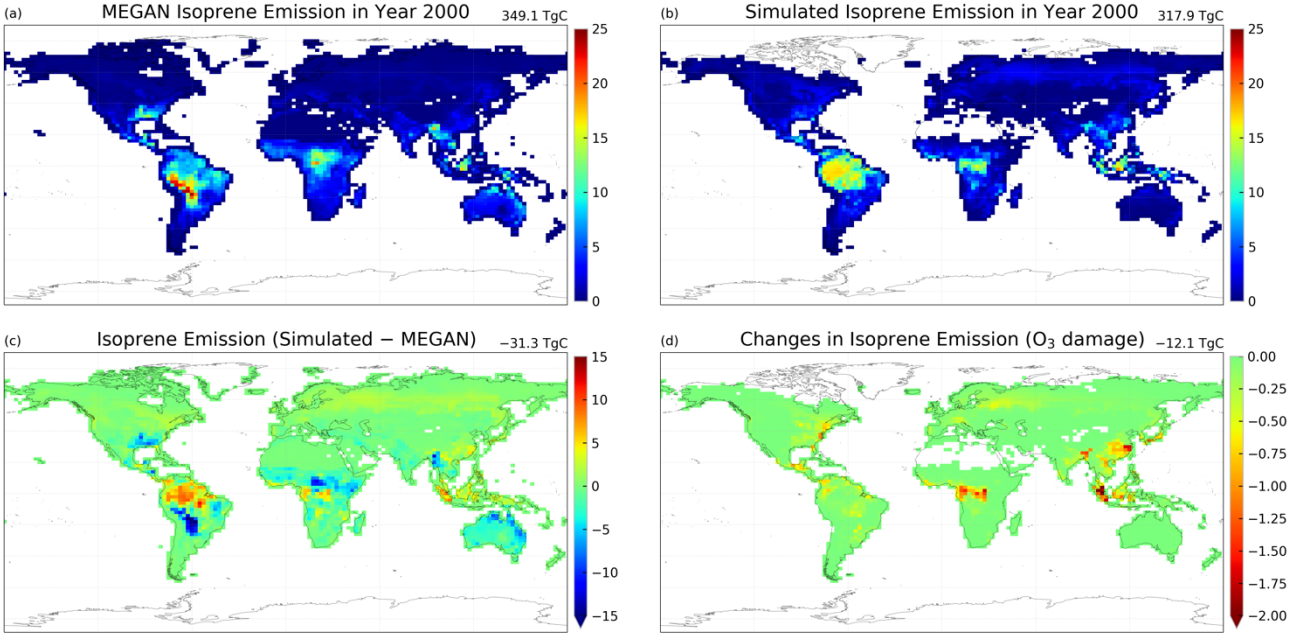

Figure 8a–d: Annual mean isoprene emission rates (g C m^{-2} yr^{-1}) for year 2000 simulated using (a) the MEGAN emission model (case 2c) and (b) the Pacifico et al. (2011) scheme coupled with the ecophysiology module without O_3 damage (case 2g), and the differences in mean isoprene emission rates due to (c) switching emission schemes (case 2g minus 2c) and (d) O_3 damage on photosynthesis, which is proportional to isoprene emission rates (case 2h minus 2g). The number on the top right corner denotes the area-weighted total of emitted isoprene. White color in the figures denotes zero value.

https://doi.org/10.5194/egusphere-2022-786
Preprint. Discussion started: 26 August 2022

In terms of GPP and O_3 depositional sink, switching isoprene emission scheme from the MEGAN emission model to a photosynthesis-based scheme by Pacifico et al. (2011), i.e., comparing case 2c to case 2g, does not change the GPP when O_3 damage is absent, as shown in Table 3. This is expected because turning off the O_3 damage scheme would interrupt the feedback pathways as shown in Fig. 1, so vegetation productivity would not be affected by atmospheric chemistry. The O_3 depositional sink is however affected because isoprene is a precursor gas of O_3. It is lowered by 5.7 Tg O_3 yr^{-1} (0.74%), due to a lower mean O_3 concentration in the tropics (Fig. 9a) where the dry deposition velocity is generally higher (Fig. 9b). The reduction in GPP due to O_3 damage does not differ as the isoprene emission scheme changes, as inferred by comparing cases 2c–d to 2g–h. This is likely due to the changes of O_3 concentration being too small to cause a significant feedback effect. Additional experiments would be required to quantify the feedback effect via the isoprene emission pathway.

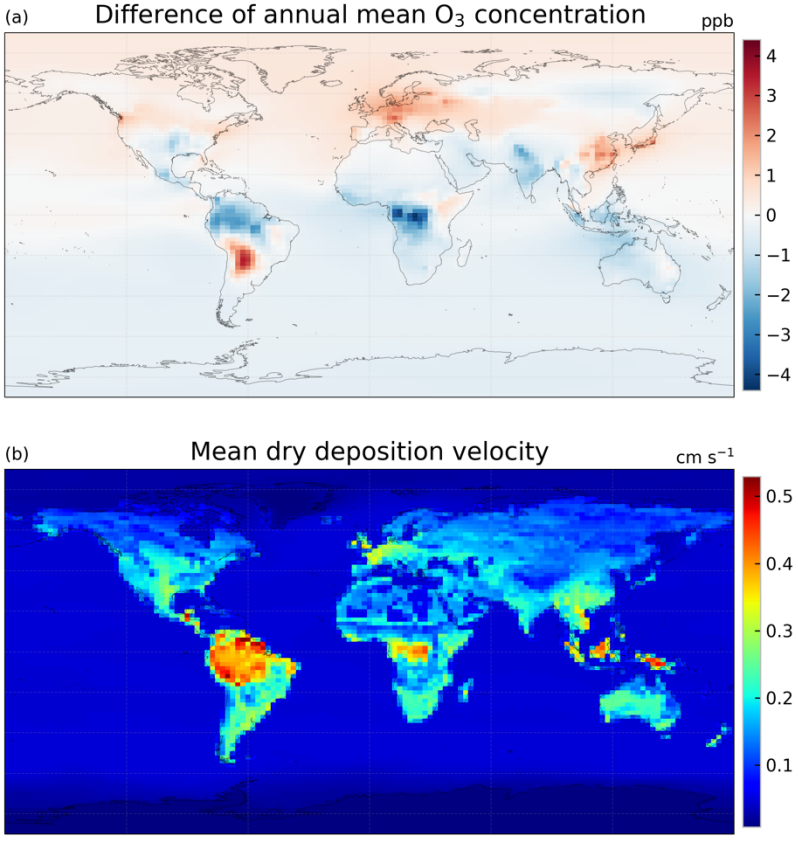

Figure 9a–b: (a) Difference in annual mean O_3 concentration (ppbv) between using the MEGAN emission model and the Pacifico et al. (2011) photosynthesis-based isoprene emission scheme (case 2g minus 2c) and (b) annual mean dry deposition velocity of O_3 (cm s^{-1}) simulated with the ecophysiology module (case 2g, and it should be very similar to case 2c).

https://doi.org/10.5194/egusphere-2022-786
Preprint. Discussion started: 26 August 2022

4 Conclusions and discussion

Tropospheric O_3 is a major air pollutant that is harmful to vegetation. It is altered by vegetation through dry deposition on plant surface and emission of BVOCs. Dry deposition to plant stomata is mainly controlled by the bulk canopy stomatal conductance g_s, which represents the openness of plant stomata in a canopy. g_s is regulated by plant physiological processes such as photosynthesis and transpiration, and thus varies strongly with environmental conditions. Moreover, plant stomata can be damaged upon exposure to O_3, resulting in reduced g_s. However, such variability is often not fully captured in CTMs. For example, the response of g_s to atmospheric or soil moisture content is missing in some models. CO_2 and O_3 concentrations also modify stomatal behavior, and in turn affect air pollutant concentrations. Therefore, ecophysiology-based approaches in modelling g_s have been suggested. They allow models to capture changes in plant stomatal and emission behaviors, which are essential in simulating biosphere–atmosphere exchange of gaseous species and O_3–vegetation interactions. In this study, we incorporate an ecophysiology module into the GEOS-Chem CTM to couple changes in atmospheric chemistry to changes in plant ecophysiological behaviors mechanistically. We then validate the simulated dry depositional velocity and concentration of O_3 against SynFlux, which is an observation-derived dataset that constrains O_3 deposition from measured water, heat, and momentum fluxes. Moreover, the module can also simulate canopy photosynthesis, which is also used for calculating isoprene emission and O_3–vegetation interactions and is itself an important indicator for ecosystem productivity and health. We investigate O_3 deposition flux and GPP under present-day and elevated CO_2 concentrations. This module provides a unique ability in evaluating the effects of pollutant deposition on air quality and plant health by allowing plant physiology to respond dynamically to changes in atmospheric chemistry and meteorological conditions.

By using a mechanistic, photosynthesis-based representation of g_s instead of the semi-empirical parameterization of Wesely (1989), the ecophysiology module reduces the overestimation in dry deposition velocity v_d of O_3 in northern summer by 0.1–0.3 cm s^{-1} across different PFTs when compared to the SynFlux observation-based dataset. The reduction is the largest for broadleaf trees and C_3 grasses. Lei et al. (2020), who coupled an integrated biosphere model to GEOS-Chem, showed that the change in annual mean v_d of O_3 due to a coupled stomatal conductance is only up to −0.15 cm s^{-1}. However, the reduction in v_d is not uniform in all seasons, but generally larger in summer, as shown in their seasonal cycle of v_d. When the comparison is restricted to the same season, our results agree with Lei et al. (2020). We further highlight that values of v_d are heavily affected by the soil moisture stress factor β_t. Representation of β_t is not very reliable in the current generation of models, and thus this is one of the main sources of uncertainties in our results. More thorough calibration of parameters related to soil water stress to more localized observations over higher spatiotemporal resolutions, as well as consideration of more soil moisture layers and distribution specific to PFTs or regions, is recommended.

Due to a decrease in dry deposition velocity of O_3, simulated O_3 concentration increases by 2–5 ppbv, amplifying the original overestimation by GEOS-Chem. Lei et al. (2020) also showed similar magnitude of changes (1–3 ppbv) in terms of annual surface O_3 concentration, and attributed the increase in O_3 concentration mostly to changes in v_d. Given the

https://doi.org/10.5194/egusphere-2022-786
Preprint. Discussion started: 26 August 2022

improvements in model performance for dry deposition velocity per se, the worsened overestimation of O_3 concentration implies greater urgency for the improvements and modifications of non-depositional processes in CTMs.

We also demonstrate that the ecophysiology module is capable of simulating O_3 deposition, plant productivity and O_3–vegetation interactions under year-2000 CO_2 (370 ppm) and elevated CO_2 (580 ppm) scenarios. Under the present-day CO_2 scenario, the global annual GPP is 119 Pg C yr^{-1}. The reduction in GPP due to O_3 damage is 4.2 Pg C yr^{-1} (3.5%) globally, and the percentage reduction can be more than 20% in the eastern US and China. This percentage roughly agrees with Yue and Unger (2015), who applied the same O_3 damage scheme from Sitch et al. (2007) to estimate global changes in GPP. An elevated CO_2 concentration leads to higher GPP through both direct CO_2 fertilization effect (+19.7 Pg C yr^{-1}) and mitigation of O_3 damage (+1.5 Pg C yr^{-1}). Monthly GPP distribution generally agrees with other models. The global O_3 deposition flux simulated under year-2000 CO_2 concentration is 772 Tg O_3 yr^{-1}, which is low relative to some multi-CTM studies (e.g., Stevenson et al., 2006; Wild, 2007). This is mostly attributable to the semi-empirical stomatal conductance used in other CTMs being generally larger than the ecophysiology-based stomatal conductance, resulting in a larger deposition flux. We also compare calculating g_s with the ecophysiology formulations to using the CO_2–g_s scaling factor suggested by Franks et al. (2013) in terms of O_3 deposition flux. The decrease in global O_3 deposition flux due to an elevated CO_2 concentration using the ecophysiology module is almost half of that using the CO_2–g_s scaling factor based on light-limited photosynthesis rate, implying that such a simple scaling approach may substantially overestimate the effect of elevated CO_2 on stomatal conductance and thus O_3 deposition.

We also implement a photosynthesis-based isoprene emission scheme in the ecophysiology module. The simulated global isoprene emission total is 317.9 Tg C yr^{-1}, which is 31.3 Tg C yr^{-1} (−9.0%) less than the values calculated using the MEGAN emission model in GEOS-Chem. The commonly accepted range is around 300–500 Tg C yr^{-1} and the simulated value is on the lower end of this range. The variability of model estimates can arise from different algorithms, vegetation presentation and other input data sources. A recent study by Weng et al. (2020) estimated a narrower range of 330–345 Tg C yr^{-1} particularly for HEMCO v2.1, which is included as the emission component of the GEOS-Chem model. Our simulated value for global isoprene emission total using the Pacifico et al. (2011) scheme is comparable. The reduction in isoprene emission due to the O_3 damage on GPP is 12.1 Tg C yr^{-1} (−3.8%), which is mainly attributable to the dry deposition pathway. All in all, the implementation of the new scheme not only serves as an alternative of the MEGAN emission model to simulate isoprene emission, but also brings new research opportunities that require isoprene emission to be mechanistically linked to plant physiology.

Limitations exist within our study. Our module only simulates ecophysiological processes directly related to photosynthesis. Unlike Lei et al. (2020), who coupled a CTM to an integrated biosphere model, we do not simulate any biogeochemical processes and ecosystem structural changes such as carbon allocation, long-term growth in biomass, litter, or soil

https://doi.org/10.5194/egusphere-2022-786
Preprint. Discussion started: 26 August 2022

decomposition. In particular, LAI does not change dynamically with climatic conditions or O_3 damage in the current model. This, however, allows our module to be computationally more efficient and perform better with respect to the reproduction of observations, when compared to other models that simulate a larger array of processes of terrestrial ecosystems extensively. The difference in computational speed from the prior GEOS-Chem v12.2.0 is barely noticeable (< 20% increase in dry deposition module run time, and < 0.001% increase in total model run time for a 6-month simulation). There are also fewer relevant ecophysiological factors contributing to variabilities in atmospheric chemistry. Thus, our module should be preferred over fully coupled Earth system models or coupling a CTM with a biosphere model (e.g., Lei et al. (2020)) if short-term (seasonal or interannual) atmosphere–biosphere exchange and air quality responses to intermittent meteorological events and stressors with a given ecosystem structure and distribution are concerned. In contrast, if long-term (e.g., multi-decadal and multi-centurial) dynamic evolution of ecosystem structure and distribution, e.g., in response to higher CO_2 level, climate change or nitrogen deposition, is an essential aspect of the study, the coupled modeling framework may be preferred.

Another limitation is that we only validate our model against SynFlux. Most of the site measurements in SynFlux are located in the US and Europe, mostly at midlatitudes. It is unclear how our results of dry deposition velocity and O_3 concentration would compare against observations in the tropics, which are relatively scarce compared to that at the midlatitudes. Moreover, C_4 grass is ignored in our results because of a lack of site observations. The module also skipped the calculation for a PFT if it does not exist within the grid cell. This prohibited us from comparing model results to observations from the few C_4 grass sites. Extending the temporal length of simulations and including other sources of site observations may solve this problem. Furthermore, utilizing the photosynthesis-based isoprene emission scheme to quantify feedback between atmospheric chemistry and vegetation via this specific pathway would be a warranted follow-up of this development. Our current set of experiments only captured modest feedbacks between O_3 concentration and vegetation productivity via both the dry deposition and isoprene emission feedback pathways (e.g., isoprene emission decreases following an O_3-induced reduction in photosynthesis), but did not consider how isoprene emission may respond immediately to acute O_3 exposure (e.g., isoprene emission increases to counteract the oxidative stress from O_3) (e.g., Loreto and Schnitzler, 2010). Comparing between different land cover inputs and evaluating the sensitivity of stomatal conductance and GPP to meteorological inputs under the new formulations using broader sources of data (e.g., satellite-derived GPP products) also warrant further investigation.

https://doi.org/10.5194/egusphere-2022-786
Preprint. Discussion started: 26 August 2022

Author contribution

JCYL wrote the source code of the ecophysiology module, conducted the model experiments and drafted the manuscript. APKT conceived the study, supervised the project, and cowrote the manuscript. JAD and CDH provided the datasets for model evaluation and supervised the writing of the manuscript.

Code and/or Data Availability

The code for the GEOS-Chem ecophysiology module and the data therein can be found in the Zenodo repository: https://doi.org/10.5281/zenodo.7017973

Acknowledgements

This work was supported by the Research Grants Council (RGC) General Research Fund (GRF; Proj. No.: 14306220) awarded to A. P. K. Tai.

https://doi.org/10.5194/egusphere-2022-786
Preprint. Discussion started: 26 August 2022

References

Ainsworth, E. A., Yendrek, C. R., Sitch, S., Collins, W. J. and Emberson, L. D.: The Effects of Tropospheric Ozone on Net Primary Productivity and Implications for Climate Change, Annual Review of Plant Biology, 63, 637–661, doi:10.1146/annurev-arplant-042110-103829, 2012.

Anenberg, S. C., Horowitz, L. W., Tong, D. Q. and West, J. J.: An estimate of the global burden of anthropogenic ozone and fine particulate matter on premature human mortality using atmospheric modeling, Environ. Health Perspect., 118, 1189–1195, doi:10.1289/ehp.0901220, 2010.

Arneth, A., Niinemets, Ü., Pressley, S., Bäck, J., Hari, P., Karl, T., Noe, S., Prentice, I. C., Serça, D., Hickler, T., Wolf, A. and Smith, B.: Process-based estimates of terrestrial ecosystem isoprene emissions: incorporating the effects of a direct CO_2-isoprene interaction, Atmos. Chem. Phys., 7, 31–53, doi:10.5194/acp-7-31-2007, 2007.

Arneth, A., Monson, R. K., Schurgers, G., Niinemets, Ü., and Palmer, P. I.: Why are estimates of global terrestrial isoprene emissions so similar (and why is this not so for monoterpenes)?, Atmos. Chem. Phys., 8, 4605–4620, https://doi.org/10.5194/acp-8-4605-2008, 2008.

Avnery, S., Mauzerall, D. L., Liu, J. and Horowitz, L. W.: Global crop yield reductions due to surface ozone exposure: 1. Year 2000 crop production losses and economic damage, Atmos. Environ., 45, 2284–2296, doi:https://doi.org/10.1016/j.atmosenv.2010.11.045, 2011.

Best, M., Pryor, M., Clark, D., Rooney, G., Essery, R., Ménard, C., Edwards, J., Hendry, M., Porson, A., Gedney, N., Mercado, L., Sitch, S., Blyth, E., Boucher, O., Cox, P., Grimmond, C. and Harding, R.: The Joint UK Land Environment Simulator (JULES), model description - Part 1: Energy and water fluxes, Geosci. Model Dev., 4, 677, doi:10.5194/gmd-4-677-2011, 2011.

Bey, I., Jacob, D., Yantosca, R., Logan, J., Field, B., Fiore, A., Li, Q., Liu, H., Mickley, L. and Schultz, M.: Global modeling of tropospheric chemistry with assimilated meteorology: Model description and evaluation, J. Geophys. Res.-Atmos., 106, 23073–23095, doi:10.1029/2001JD000807, 2001.

Bonan, G.: Ecological Climatology: Concepts and Applications, 3rd ed., Cambridge University Press, Cambridge, 2015.

Clark, D., Mercado, L., Sitch, S., Jones, C., Gedney, N., Best, M., Pryor, M., Rooney, G., Essery, R., Blyth, E., Boucher, O., Harding, R., Huntingford, C. and Cox, P.: The Joint UK Land Environment Simulator (JULES), model description - Part 2: Carbon fluxes and vegetation dynamics, Geosci. Model Dev., 4, 701, doi:10.5194/gmd-4-701-2011, 2011.

Collatz, G. J., Ball, J. T., Grivet, C. and Berry, J. A.: Physiological and environmental regulation of stomatal conductance, photosynthesis and transpiration: a model that includes a laminar boundary layer, Agr. Forest Meteorol., 54, 107–136, doi:10.1016/0168-1923(91)90002-8, 1991.

Collatz, G., Ribas-Carbo, M. and Berry, J.: Coupled Photosynthesis-Stomatal Conductance Model for Leaves of C_4 Plants, Aust. J. Plant Physiol., 19, 519–538, 1992.

https://doi.org/10.5194/egusphere-2022-786
Preprint. Discussion started: 26 August 2022

Cox, P. M., Huntingford, C. and Harding, R. J.: A canopy conductance and photosynthesis model for use in a GCM land surface scheme, J. Hydrol., 212, 79–94, doi:10.1016/S0022-1694(98)00203-0, 1998.

De Kauwe, M. G., Kala, J., Lin, Y.-S., Pitman, A. J., Medlyn, B. E., Duursma, R. A., Abramowitz, G., Wang, Y.-P. and Miralles, D. G.: A test of an optimal stomatal conductance scheme within the CABLE land surface model, Geosci. Model Dev., 8, 431, doi:10.5194/gmd-8-431-2015, 2015.

Ducker, J. A., Holmes, C. D., Keenan, T. F., Fares, S., Goldstein, A. H., Mammarella, I., Munger, J. W. and Schnell, J.: Synthetic ozone deposition and stomatal uptake at flux tower sites, Biogeosciences, 15, 5395–5413, doi:10.5194/bg-15-5395-2018, 2018.

Emberson, L. D., Kitwiroon, N., Beevers, S., Büker, P. and Cinderby, S.: Scorched Earth: how will changes in the strength of the vegetation sink to ozone deposition affect human health and ecosystems?, Atmos. Chem. Phys., 13, 6741, doi:10.5194/acp-13-6741-2013, 2013.

Franks, P. J. and Farquhar, G. D.: A relationship between humidity response, growth form and photosynthetic operating point in C 3 plants, Plant, Cell Environ., 22, 1337–1349, doi:10.1046/j.1365-3040.1999.00494.x, 1999.

Franks, P. J., Adams, M. A., Amthor, J. S., Barbour, M. M., Berry, J. A., Ellsworth, D. S., Farquhar, G. D., Ghannoum, O., Lloyd, J., Mcdowell, N., Norby, R. J., Tissue, D. T. and Caemmerer, S.: Sensitivity of plants to changing atmospheric CO_2 concentration: from the geological past to the next century, New Phytol., 197, 1077–1094, doi:10.1111/nph.12104, 2013.

Gelaro, R., McCarty, W., Suárez, M. J., Todling, R., Molod, A., Takacs, L., Randles, C. A., Darmenov, A., Bosilovich, M. G., Reichle, R., Wargan, K., Coy, L., Cullather, R., Draper, C., Akella, S., Buchard, V., Conaty, A., da Silva, A. M., Gu, W., Kim, G.-K., Koster, R., Lucchesi, R., Merkova, D., Nielsen, J. E., Partyka, G., Pawson, S., Putman, W., Rienecker, M., Schubert, S. D., Sienkiewicz, M. and Zhao, B.: The Modern-Era Retrospective Analysis for Research and Applications, Version 2 (MERRA-2), J. Climate, 30, 5419–5454, doi:10.1175/JCLI-D-16-0758.1, 2017.

Guenther, A. B., Jiang, X., Heald, C. L., Sakulyanontvittaya, T., Duhl, T., Emmons, L. K. and Wang, X.: The Model of Emissions of Gases and Aerosols from Nature version 2.1 (MEGAN2.1): an extended and updated framework for modeling biogenic emissions, Geosci. Model Dev., 5(6), 1471–1492, doi:10.5194/gmd-5-1471-2012, 2012.

Hoesly, R. M., Smith, S. J., Feng, L., Klimont, Z., Janssens-Maenhout, G., Pitkanen, T., Seibert, J. J., Vu, L., Andres, R. J., Bolt, R. M., Bond, T. C., Dawidowski, L., Kholod, N., Kurokawa, J.-I., Li, M., Liu, L., Lu, Z., Moura, M. C. P., O'Rourke, P. R. and Zhang, Q.: Historical (1750–2014) anthropogenic emissions of reactive gases and aerosols from the Community Emissions Data System (CEDS), Geosci. Model Dev., 11, 369–408, doi:10.5194/gmd-11-369-2018, 2018.

Huang, L., McDonald-Buller, E. C., McGaughey, G., Kimura, Y. and Allen, D. T.: The impact of drought on ozone dry deposition over eastern Texas, Atmos. Environ., 127, 176–186, doi:https://doi.org/10.1016/j.atmosenv.2015.12.022, 2016.

Huntingford, C., Oliver, R. J., Mercado, L. M., and Sitch, S.: Technical note: A simple theoretical model framework to describe plant stomatal "sluggishness" in response to elevated ozone concentrations, Biogeosciences, 15, 5415–5422, https://doi.org/10.5194/bg-15-5415-2018, 2018.

https://doi.org/10.5194/egusphere-2022-786
Preprint. Discussion started: 26 August 2022

Jacob, D. J. and Winner, D. A.: Effect of climate change on air quality, Atmos. Environ., 43, 51-63, doi:10.1016/j.atmosenv.2008.09.051, 2009.

Jarvis, P. G.: Interpretation of Variations in Leaf Water Potential and Stomatal Conductance Found in Canopies in Field, Philosophical Transactions of the Royal Society of London Series B-Biological Sciences, 273, 593-610, doi:DOI 10.1098/rstb.1976.0035, 1976.

Kavassalis, S. C. and Murphy, J. G.: Understanding ozone-meteorology correlations: A role for dry deposition, Geophys. Res. Lett., 44, 2922–2931, doi:10.1002/2016GL071791, 2017.

Keller, C. A., Long, M. S., Yantosca, R. M., Da Silva, A. M., Pawson, S., and Jacob, D. J.: HEMCO v1.0: a versatile, ESMF-compliant component for calculating emissions in atmospheric models, Geosci. Model Dev., 7, 1409–1417, https://doi.org/10.5194/gmd-7-1409-2014, 2014.

Lei, Y., Yue, X., Liao, H., Gong, C. and Zhang, L.: Implementation of Yale Interactive terrestrial Biosphere model v1.0 into GEOS-Chem v12.0.0: a tool for biosphere–chemistry interactions, Geosci. Model Dev., 13, 1137–1153, doi:10.5194/gmd-13-1137-2020, 2020.

Leuning, R.: A critical appraisal of a combined stomatal-photosynthesis model for C_3 plants, Plant Cell Environ., 18, 339–355, doi:10.1111/j.1365-3040.1995.tb00370.x, 1995.

Lombardozzi, D., Levis, S., Bonan, G., Hess, P. G. and Sparks, J. P.: The Influence of Chronic Ozone Exposure on Global Carbon and Water Cycles, J. Climate, 28, 292–305, doi:10.1175/JCLI-D-14-00223.1, 2015.

Loreto, F. and Schnitzler, J.-P., Abiotic stresses and induced BVOCs, Trends in Plant Sci., 15, 154-156, doi: 10.1016/j.tplants.2009.12.006, 2010.

Medlyn, B. E., Duursma, R. A., Eamus, D., Ellsworth, D. S., Prentice, I. C., Barton, C. V. M., Crous, K. Y., De Angelis, P., Freeman, M. and Wingate, L.: Reconciling the optimal and empirical approaches to modelling stomatal conductance, Global Change Biol., 17, 2134–2144, doi:10.1111/j.1365-2486.2010.02375.x, 2011.

Monson, R. and Baldocchi, D.: Terrestrial Biosphere-Atmosphere Fluxes, Cambridge University Press, Cambridge., 2014.

Pacifico, F., Harrison, S. P., Jones, C. D., Arneth, A., Sitch, S., Weedon, G. P., Barkley, M. P., Palmer, P. I., Serça, D., Potosnak, M., Fu, T.-M., Goldstein, A., Bai, J., and Schurgers, G.: Evaluation of a photosynthesis-based biogenic isoprene emission scheme in JULES and simulation of isoprene emissions under present-day climate conditions, Atmos. Chem. Phys., 11, 4371–4389, doi:10.5194/acp-11-4371-2011, 2011.

Possell, M. and Hewitt, C. N.: Isoprene emissions from plants are mediated by atmospheric CO_2 concentrations, Global Change Biol., 17, 1595–1610, doi:10.1111/j.1365-2486.2010.02306.x, 2011.

Prather, M. J. and Ehhalt, D.: Atmospheric Chemistry and Greenhouse Gases, edited by J. T. Houghton, Y. Ding, and D. J. Griggs, Cambridge University Press, Cambridge., 2001.

Raoult, N. M., Jupp, T. E., Cox, P. M. and Luke, C. M.: Land-surface parameter optimisation using data assimilation techniques: the adJULES system V1.0, Geosci. Model Dev., 9, 2833, doi:10.5194/gmd-9-2833-2016, 2016.

https://doi.org/10.5194/egusphere-2022-786
Preprint. Discussion started: 26 August 2022

Ronan, A. C., Ducker, J. A., Schnell, J. L., and Holmes, C. D.: Have improvements in ozone air quality reduced ozone uptake into plants? Elem Sci Anth, 8, 2, doi:10.1525/elementa.399, 2020.

Sadiq, M., Tai, A. P. K., Lombardozzi, D. and Val Martin, M.: Effects of ozone–vegetation coupling on surface ozone air quality via biogeochemical and meteorological feedbacks, Atmos. Chem. Phys., 17, 3055–3066, doi:10.5194/acp-17-3055-2017, 2017.

Sanderson, M. G., Jones, C. D., Collins, W. K., Johnson, C. E. and Derwent, R. G.: Effect of Climate Change on Isoprene Emissions and Surface Ozone Levels, Geophys. Res. Lett., 30, 1936, doi:10.1029/2003GL017642, 2003.

Sanderson, M. G., Collins, W. J., Hemming, D. L. and Betts, R. A.: Stomatal conductance changes due to increasing carbon dioxide levels: Projected impact on surface ozone levels, Tellus B: Chemical and Physical Meteorology, 59, 404–411, doi:10.1111/j.1600-0889.2007.00277.x, 2007.

Sellers, P. J., Randall, D. A., Collatz, G. J., Berry, J. A., Field, C. B., Dazlich, D. A., Zhang, C., Collelo, G. D. and Bounoua, L.: A Revised Land Surface Parameterization (SiB2) for Atmospheric GCMs. Part I: Model Formulation, J. Climate, 9, 676–705, 1996.

Sitch, S., Cox, P. M., Collins, W. J. and Huntingford, C.: Indirect radiative forcing of climate change through ozone effects on the land-carbon sink, Nature, 448, 791, doi:10.1038/nature06059, 2007.

Slevin, D., Tett, S. F. B., Exbrayat, J.-F., Bloom, A. A. and Williams, M.: Global evaluation of gross primary productivity in the JULES land surface model v3.4.1, Geosci. Model Dev., 10, 2651, doi:10.5194/gmd-10-2651-2017, 2017.

Stevenson, D. S., Dentener, F. J., Schultz, M. G., Ellingsen, K., van Noije, T. P. C., Wild, O., Zeng, G., Amann, M., Atherton, C. S., Bell, N., Bergmann, D. J., Bey, I., Butler, T., Cofala, J., Collins, W. J., Derwent, R. G., Doherty, R. M., Drevet, J., Eskes, H. J., Fiore, A. M., Gauss, M., Hauglustaine, D. A., Horowitz, L. W., Isaksen, I. S. A., Krol, M. C., Lamarque, J.-F., Lawrence, M. G., Montanaro, V., Müller, J.-F., Pitari, G., Prather, M. J., Pyle, J. A., Rast, S., Rodriguez, J. M., Sanderson, M. G., Savage, N. H., Shindell, D. T., Strahan, S. E., Sudo, K. and Szopa, S.: Multimodel ensemble simulations of present-day and near-future tropospheric ozone, J. Geophys. Res., 111, doi:10.1029/2005JD006338, 2006.

Tai, A. P. K., Mickley, L. J., Heald, C. L. and Wu, S.: Effect of CO2 inhibition on biogenic isoprene emission: Implications for air quality under 2000 to 2050 changes in climate, vegetation, and land use, Geophys. Res. Lett., 40, 3479–3483, doi:10.1002/grl.50650, 2013.

Tai, A. P. K., Martin, M. V. and Heald, C. L.: Threat to future global food security from climate change and ozone air pollution, Nature Climate Change, 4, 817–821, doi:10.1038/nclimate2317, 2014.

Tai, A. P. K. and Val Martin, M.: Impacts of ozone air pollution and temperature extremes on crop yields: Spatial variability, adaptation and implications for future food security, Atmos. Environ., 169, 11–21, doi:https://doi.org/10.1016/j.atmosenv.2017.09.002, 2017.

https://doi.org/10.5194/egusphere-2022-786
Preprint. Discussion started: 26 August 2022

Travis, K. R., Jacob, D. J., Fisher, J. A., Kim, P. S., Marais, E. A., Zhu, L., Yu, K., Miller, C. C., Yantosca, R. M., Sulprizio, M. P., and Thompson, A.M. Why do models overestimate surface ozone in the southeastern United States? Atmos. Chem. Phys., 16(21), 13561-13577, doi:10.5194/acp-16-13561-2016, 2016.

Trugman, A. T., Medvigy, D., Mankin, J. S. and Anderegg, W. R. L.: Soil Moisture Stress as a Major Driver of Carbon Cycle Uncertainty, Geophys. Res. Lett., 45, 6495–6503, doi:10.1029/2018GL078131, 2018.

Unger, N.: Isoprene emission variability through the twentieth century, J. Geophys. Res.-Atmos., 118, 13,606-13,613, doi:10.1002/2013JD020978, 2013.

Wang, L., Tai, A. P. K., Tam, C. Y., Sadiq, M., Wang, P., and Cheung, K. K. W.: Impacts of future land use and land cover change on mid-21st-century surface ozone air quality: distinguishing between the biogeophysical and biogeochemical effects, Atmos. Chem. Phys., 20, 11349-11369, doi:10.5194/acp-20-11349-2020, 2020.

Weng, H., Lin, J., Martin, R., Millet, D., Jaeglé, L., Ridley, D., Keller, C., Li, C., Du, M., Meng, J.: Global high-resolution emissions of soil NO_x, sea salt aerosols, and biogenic volatile organic compounds, Sci Data 7, 148, doi.org:10.1038/s41597-020-0488-5, 2020.

Wesely, M. L.: Parameterization of surface resistances to gaseous dry deposition in regional-scale numerical models, Atmos. Environ., 23, 1293–1304, doi:10.1016/0004-6981(89)90153-4, 1989.

Wild, O.: Modelling the global tropospheric ozone budget: exploring the variability in current models, Atmos. Chem. Phys., 7, 2643–2660, doi:10.5194/acp-7-2643-2007, 2007.

Wong, A. Y. H., Geddes, J. A., Tai, A. P. K. and Silva, S. J.: Importance of dry deposition parameterization choice in global simulations of surface ozone, Atmos. Chem. Phys., 19, 14365–14385, doi:10.5194/acp-19-14365-2019, 2019.

Young, P.J., Naik, V., Fiore, A.M., Gaudel, A., Guo, J., Lin, M.Y., Neu, J.L., Parrish, D.D., Rieder, H.E., Schnell, J.L., Tilmes, S., Wild, O., Zhang, L., Ziemke, J.R., Brandt, J., Delcloo, A., Doherty, R.M., Geels, C., Hegglin, M.I., Hu, L., Im, U., Kumar, R., Luhar, A., Murray, L., Plummer, D., Rodriguez, J., Saiz-Lopez, A., Schultz, M.G., Woodhouse, M.T. and Zeng, G.: Tropospheric Ozone Assessment Report: Assessment of global-scale model performance for global and regional ozone distributions, variability, and trends. Elem Sci Anth, 6(1), 10, doi:10.1525/elementa.265, 2018.

Yuan, H., Dai, Y., Xiao, Z., Ji, D. and Shangguan, W.: Reprocessing the MODIS Leaf Area Index products for land surface and climate modelling, Remote Sens. Environ., 115, 1171–1187, doi:https://doi.org/10.1016/j.rse.2011.01.001, 2011.

Yue, X. and Unger, N.: The Yale Interactive terrestrial Biosphere model version 1.0: description, evaluation and implementation into NASA GISS ModelE2, Geosci. Model Dev., 8, 2399–2417, doi:10.5194/gmd-8-2399-2015, 2015.

Zhang, L., Brook, J. R. and Vet, R.: A revised parameterization for gaseous dry deposition in air-quality models, Atmos. Chem. Phys., 3, 2067–2082, doi:10.5194/acp-3-2067-2003, 2003.

Zhou, S. S., Tai, A. P. K., Sun, S., Sadiq, M., Heald, C. L. and Geddes, J. A.: Coupling between surface ozone and leaf area index in a chemical transport model: strength of feedback and implications for ozone air quality and vegetation health, Atmos. Chem. Phys., 18, 14133–14148, doi:10.5194/acp-18-14133-2018, 2018.